Development of Silane Modified Inorganic Membranes for Gas and Vapor Separations

by

Kenneth C. McCarley

A thesis submitted to the Faculty and Board of Trustees of the Colorado School of Mines in partial fulfillment of the requirements for the degree of Doctor of Philosophy (Chemical and Petroleum Refining Engineering).

Golden, Colorado

Date 11 - 5 - 99

Signed: Ken McCarley

Kenneth C. McCarley

Approved J Douglas Way

Dr. J. Douglas Way
Thesis Advisor

Golden, Colorado

Date 11/8/99

Robert Baldwin

Dr. Robert Baldwin
Professor and Head, Department of Chemical Engineering

ABSTRACT

Novel organic/inorganic gas-separation membranes were fabricated by modification of mesoporous γ-alumina ultrafilters with octadecylsilane (ODS) and (heptadecafluoro-1,1,2,2-tetrahydrodecyl)-trichlorosilane (HDFS). We demonstrated that changing the chemistry of the silane coupling agent changed membrane selectivity. Based on ellipsometry measurements and XPS analysis, our hypothesis is that the membranes were composed of a very thin, approximately 11 nm, layer grafted to the surface of the mesoporous substrate. However, the microstructure of the silane layer is not well understood.

Pure gas permeance of the alumina membrane decreased by 2 to 3 orders of magnitude after modification with ODS. Permeance of the ODS membrane was history dependent, however the permeance could be recovered by rinsing in toluene and drying at 333 K, or by exposure to flowing N_2 with a pressure drop across the membrane of approximately 5.0 psi. The pure gas permeance fit an exponential relationship with critical temperature that was consistent with transport based on preferential adsorption and solution diffusion. Also, a model for surface diffusion enhanced permeation provided a parametric fit to the pure gas permeance of the ODS membrane.

The pure gas permeance of the HDFS membrane decreased by 3 to 4 orders of magnitude compared to the unmodified sample. The HDFS layer was not thermally

stable, as indicated by irreversible changes in permeance and selectivity after exposure to temperatures up to 353 K. In contrast to the ODS membrane, pure gas permeance of the HDFS membrane followed an exponential relationship with the inverse of the kinetic diameter of the gas. Therefore, the dominant transport mechanism transport was configurational diffusion, however the transport of CO_2 was also enhanced by preferential adsorption.

After silane modification both membranes exhibited *reverse selectivity*, or selectivity for heavier gases such as CO_2 and n-C_4H_{10}, over lighter gases such as H_2, N_2 CH_4 and C_2H_6. Reverse selectivities were measured as high as 48 for n-C_4H_{10}/N_2 and 24 for n-C_4H_{10}/CH_4. Most significantly, the order of selectivity for CO_2 over hydrocarbons changed between the ODS and HDFS membranes. Pure gas selectivities for CO_2/n-C_4H_{10} were 0.107 for the ODS membrane and 13.5, or over 100 times greater, for the HDFS membrane. This change in order of selectivity was a convincing demonstration of the effect of silane modification on membrane performance.

Pervaporation experiments were performed to screen the ODS, HDFS and two zeolite (silicalite and ZSM-5) membranes for the separation of xylene isomers. Selectivities for o-xylene/p-xylene as high as 1.5 and 2.4 were observed for the HDFS and ZSM-5 membranes, respectively. Selectivity for the most polar isomer, o-xylene, was enhanced by using membranes that offered a more polar environment.

TABLE OF CONTENTS

Page

Page

LIST OF FIGURES

Page

LIST OF TABLES

ACKNOWLEDGMENTS

This work was supported in part by Chevron Research and Technology Company and DOE-Basic Energy Sciences Grant # DE-FG03-93ER14363.

I wish to thank my advisor Dr. J.D.Way, and my committee members: Dr. Annette Bunge, Dr. Mark Eberhart, Dr. Jim Ely, and Dr. Tim Ohno for their advice, patience and valuable suggestions. I would also like to thank Dr. T. Ohno for performing the XPS analysis, Dr. John Nicholas (Battelle, Pacific Northwest Laboratories) and Dr. Mark Eberhart for suggestions concerning quantum mechanical calculations, Dr. Curt Munson and Dr. Don Mohr (Chevron Research and Technology Company) for there advice concerning membrane developments. I would also like to give thanks to Dr. Kelly McCarley for proof reading this thesis.

To Kelly, Katie and Kenny

Chapter 1

Introduction

The subject of this research was conceived during our (Professor Way's membrane separations group) study of the effects of molecular interactions between gases and surfaces on transport phenomena through microporous membrane materials. At the time, our subject was enhanced permeance of gases due to interactions with hydroxyl groups on the surface of microporous silica memrbanes, as discussed in Appendix 1. During our research, papers on surface modification of inorganic membranes and the development of stationary phases for the separation of aromatic isomers by chromatography, led us to become interested in the fabrication of membranes based on the same principles applied to the development of high performance chromatography.

1.1 The Membrane Industry

Separation processes account for 40-70% of both capital and operating expenses in the chemical processing industries and the development of more efficient technologies are essential to significantly reduce costs [1]. A 1987 study by the United States Department of Energy showed that the total energy consumption for separation processes by the chemical process industry in the United Sates was over 5 Quads per year (1 Quad = 10^{15} Btu, equivalent to 170 million barrels of oil) [1-3]. Distillation alone consumed about 2.4 quads per year, or about 100,000 barrels of oil per day. The same study predicted that nearly 20% of that energy could be saved through increased use of membrane separations systems in chemical and petroleum processing [2,3].

In 1987 Keller asked 16 chemical separations experts to grade several separations processes based on technological advancement, or "technical maturity", and extent of commercial application, "use maturity" [4]. Figure 1-1 shows the results of Keller's survey of maturity graded from 0-100%, where 0 indicates conception of the process and 100 is the limiting asymptote for advancement of each technology or the possible number of applications. Although there is an obvious element of uncertainty in this assessment, it provides valuable insight into the industry. For example, distillation, which lies in the upper right corner of the plot, is the most widely used separation process in industry and there is little room for technological advancement. On the other hand, membrane technology, placed in the lower left half of the chart, is far from its technological asymptote and is not widely used. Although membrane technology has advanced considerably since this survey and the worldwide markets for membranes have increased from about \$1.6 billion to \$3.9 billion since 1986, some areas of membrane research are still under developed [1]. For instance, in 1996 high performance membranes for gas separations still only amounted to about \$100 million of the market, while the less

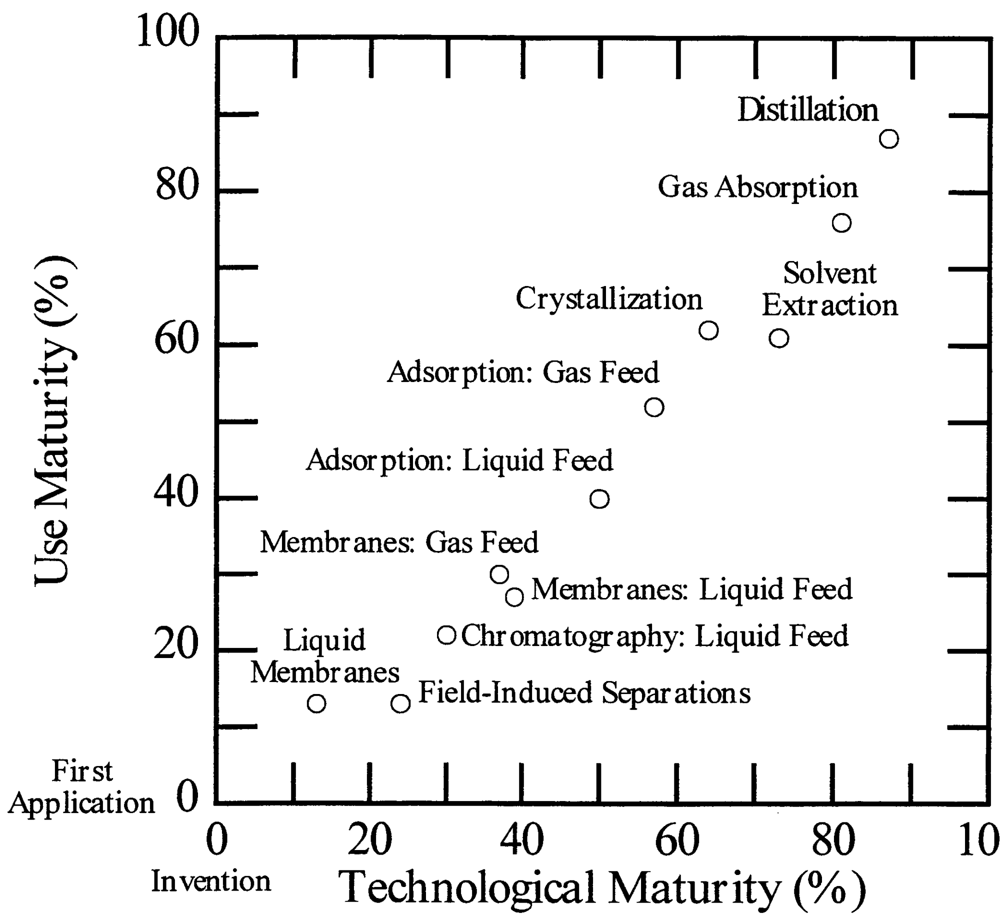

Figure 1-1: A comparison of technological and use maturity of separation processes. Maturity in technology and use are expected to reach 100% asymptotically [4].

complicated microfiltration membranes make up about \$1.5 billion of the market [1]. Based on the present level of the membrane market and along with DOE's predicted energy savings, research and development of membrane separations for the chemical processing industry is currently in high demand.

1.2 What is a Membrane?

Membranes are barriers that control the rate of chemical permeation between two phases. If certain compounds in a mixture permeate through the membrane (material) at higher rates than others, then a chemical separation is achieved. Membrane materials are specifically engineered for chemical separations based on differences in molecular size and shape, and chemical affinity.

Gas separations are typically performed with a feed mixture at high pressure that provides driving force for flux through the membrane. The permeation of gases through membranes is often expressed in terms of *permeance* (P_i), which is defined as the flux (J_i) of species i normalized by the partial pressure driving force (Δp_i) across the membrane, as given in equation (1.1):

$$P_i = \frac{J_i}{\Delta p_i} \tag{1.1}$$

Pure gas permeances are also measured as a baseline for comparison between membranes and for the analysis of transport mechanisms. Selectivity can be defined in terms of pure or mixed gases as the ratio of the gas permeances:

$$\alpha_{i/j} = \frac{P_i}{P_j} \tag{1.2}$$

Flux is not always linear with pressure or constant with temperature, therefore permeance and selectivity are only useful for comparison at similar conditions.

1.3 Materials and Transport

Membranes are commonly divided into two main categories depending on whether they are made of a *porous* or *dense* (*nonporous*) material. Examples of porous membrane materials designed for chemical (gas or liquid) separations are zeolites[5,6], porous glass [7] and porous polymer structures [8]. Examples of dense membrane materials are thin film palladium [9], silicone and polyethylene [8]. Classification of membranes are typically based on the microstructure and the description of the transport mechanisms that responsible for their selectivity during gas separations.

Figure 1-2 is a schematic representation of the transport mechanisms involved in selective transport of gases and vapors through membranes [5]. Transport mechanisms that are not selective, such as viscous flow and molecular diffusion, are not included in Figure 1-2. Knudsen diffusion occurs in porous membranes when the mean free path the gas is

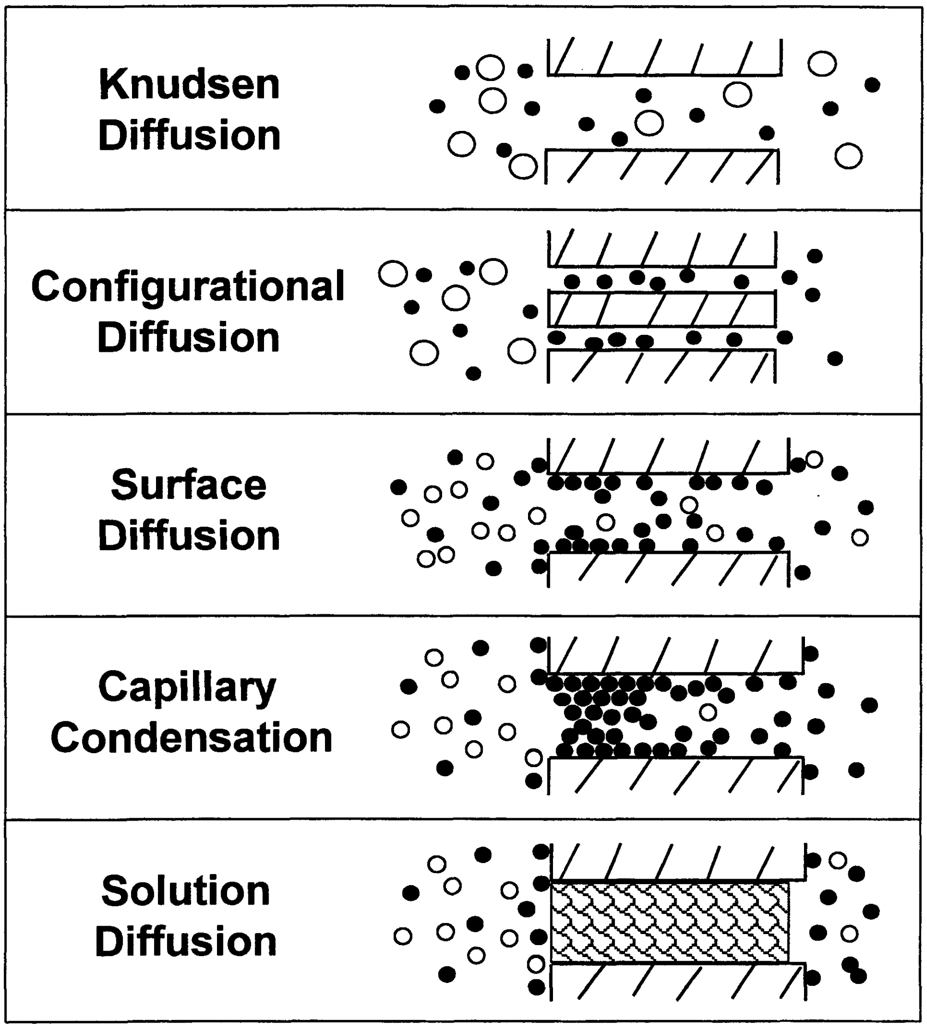

Figure 1-2: Schematic representation of the transport mechanisms responsible for selectivity in membranes.

larger than the mean pore diameter of the membrane (20-1000 Å). The rate of permeation by Knudsen diffusion is proportional to the inverse of the square root of the molecular weight. Therefore, the theoretical Knudsen selectivity, α, can be calculated as the square root of the ratio of the inverse ratio of the molecular weights of species i and j, as given below [5]:

$$\alpha_{i/j} = \sqrt{\frac{M_j}{M_i}} \tag{1.3}$$

Selectivities obtained through Knudsen diffusion are not high, even for gas mixtures with a large range in molecular weights. For example, the theoretical Knudsen selectivity for H_2/n-C_4H_{10} is 5.4.

Configurational diffusion occurs in molecular sieve and/or microporous membranes that have pore sizes that are comparable to the kinetic diameter of gases (3-15 Å). Selectivity is based on discrimination of gases by molecular shape and size. Very high selectivities can be achieved with this mechanism. For example, selectivities for H_2/i-C_4H_{10} of over 100 have been observed for microporous silica and MFI zeolite membranes, and n-C_4H_{10}/i-C_4H_{10} of over 50 have been observed for MFI zeolite membranes.

Selectivity for gases based on surface diffusion, capillary condensation and solution diffusion is dependent on the adsorption phenomena of a particular gas with respect to the membrane material [5,10]. Surface diffusion and capillary condensation occur in porous materials in parallel with other transport mechanisms, such as Knudsen diffusion and configurational diffusion [5-7]. Gases that are non-condensable or close to critical temperature adsorb and diffuse along surfaces at low concentrations. Gases that are closer to their saturation vapor pressure exhibit high selectivities through vapor phase flow with multilayer adsorption and capillary condensation, however it is often at the cost of very low (liquid) permeation rates.

Solution diffusion occurs in dense materials, such as polymers, and the permeance is a product of the solubility and diffusivity of the gas with respect to the membrane material [8]. Figure 1-2 illustrates solution diffusion, in parallel with porous diffusion, through a dense material deposited inside of a pore. Alternatively, solution diffusion could also take place in a dense layer deposited as a thin film on top of a porous material.

In many cases, surface flow enhanced diffusion and solution diffusion result in selectivities for heavier, more condensable gases, over lighter gases in a mixture, which is defined as *reverse selectivity*. Reverse selectivities as high as 94 for n-C_4H_{10}/H_2 have been observed for nanoporous carbon membranes [11]. Many materials have been developed for chromatographic separations by attaching functional groups (i.e., molecules that interact with specific compounds) to the surface of porous inorganic materials with silane coupling agents. This concept has been demonstrated extensively by developers of column packing materials for high performance liquid chromatography (HPLC), capillary gas chromatography and solid phase extraction [12-14].

1.4 Thesis Objectives and Organization

In this thesis we showed the feasibility of fabricating reverse selective gas separation membranes through silane modification of mesoporous alumina with organosilanes. Most significantly, this work demonstrated that the selectivity of the membrane could be tailored intentionally for specific separations by choosing an appropriate functional group. We showed an increase in selectivity for CO_2 over hydrocarbons by comparison of membranes modified with a fluorinated-alkylsilane [15,16] in place of an alkylsilane [16,17].

The specific objectives of this research were:

i. To develop gas separation membranes by modifying the surface of commercially available mesoporous alumina substrates with silane coupling agents. (Chapter 2 and 3)

ii. To demonstrate a change in selectivity for CO_2 over hydrocarbons by surface modified membranes by changing the chemistry of the silane coupling agent. (Chapter 3)

iii. To investigate the transport phenomena through a silane modified membrane using a surface diffusion enhanced permeation (SEP) model. (Chapter 2)

v. To perform a conceptual study, and screening of membranes, for the separation of xylene isomers by pervaporation. (Chapter 4)

1.5 Nomenclature

J_i Flux of species *i* ($scc \cdot s^{-1} \cdot cm^{-2}$)

M_i Molecular weight of species *i* (g/mole)

Δp_i Partial pressure driving force for species *i* (psi)

P_i Permeance of species *i* ($scc \cdot s^{-1} \cdot cm^{-2} \cdot cmHg^{-1}$)

Greek Symbols

$\alpha_{i/j}$ Selectivity for species *i* over species *j*

1.6 References

1 J. L. Humphrey and G. E. Keller, *Separation Process Technology* (McGraw-Hill, New York, 1997).

2 D. O. o. I. Programs, (United States Department of Energy, Springfield, 1987).

3 D. W. Schaefer, *MRS Bulletin* (1994).

4 G. E. Keller, *American Institute of Chemical Engineers Monograph Series* **17** (1987).

5 A. J. Burggraaf, in *Fundamentals of Inorganic Membrane Science and Technology*, edited by A. J. Burggraaf and L. Cot (Elsevier Science B.V., 1996), pp. 331-431.

6 A. J. Burggraaf, *Journal of Membrane Science* **155,** 45-65 (1999).

7 M. H. Hassan, Ph.D., Oregon State University, 1994.

8 R. E. Kesting, *Synthetic Polymeric Membranes* (McGraw-Hill, New York, 1971).

9 S. N. Paglieri, K. Y. Foo, J. D. Way, J. P. Collins, and D. L. Harper-Nixon, *Industrial & engineering chemistry research* **38,** 1925 (1999).

10 S.-T. Hwang and K. Kammermeyer, *Membranes in Separations* (John Wiley and Sons, New York, 1975).

11 M. B. Rao and S. Sircar, *Journal of Membrane Science* **85,** 253-264 (1993).

12 B. Buszewski, R. M. Gadzala-Kopciuch, M. Markuszewski, and R. Kaliszan, *Analytical Chemistry* **69,** 3277-3284 (1997).

13 M. Ho, M. Cai, and J. E. Pemberton, *Analytical Chemistry* **69,** 2613-2616 (1997).

14 A. L. Jadhav, K. P. Naikwadi, S. Rokushika, H. Hatano, and M. Ohshima, *Journal of High Resolution Chromatography & Chromatography Communications* **10,** 77-81 (1987).

15 J. R. Miller and W. J. Koros, *Separation Science and Technology* **25,** 1257 - 1280 (1990).

16 P. Mejean, A. Collet, M. Viguier, A. Sivade, D. Bourret, and A. Larbot, in *ICIM 5* (Japan, 1998), pp. 176-179.

17 C. Leger, H. D. L. Lira, and R. Paterson, *Journal of Membrane Science* **120,** 187-195 (1996).

Chapter 2

Development of a Model Surface Flow Membrane by Modification of Porous γ-Alumina with Octadecyltrichlorosilane

2.1 Introduction

Membranes discriminate between molecules through differences in their rates of diffusion due to surface and configurational interactions. Separations due to configurational interactions are achieved when the pore size, or free volume, in a rigid matrix is small enough to differentiate between molecules based on shape and/or size. Surface interactions determine the amount of pore loading and surface flow that act in parallel with other transport mechanisms.

Many inorganic microporous and mesoporous materials have been developed for chemical separations and the surface chemistry of these materials can be modified for specific chemical separations. This concept has been demonstrated extensively by developers of column packing materials for high performance liquid chromatography (HPLC), capillary gas chromatography and solid phase extraction [1-3].

Though chromatography is a batch process, as opposed to a continuous process that is desired for membranes, the phenomena employed for the separation of chemicals are fundamentally similar. Packing materials comprised of chemically modified silicas are commercially available and preparation of these materials is a popular area of research. Functional stationary phases, such as C_{18}, C_8, C_2, NH_2, CN, DIOL, etc. [3], are typically grafted covalently to silica surfaces using chlorosilanes or alkoxysilanes. Stationary phases under development include a variety of new functional groups and structures, including brush layers, polymer layers and liquid crystalline phases [3-6]. As HPLC packings, these new materials are capable of performing difficult separations, such as positional isomers and optical isomers of aromatic hydrocarbons.

Modification of the functional groups on inorganic membranes for gas and liquid separations has also been studied. Okubo and Inoue modified porous silica with a 3 nm pore diameter by esterfication of the hydroxylated surface with three alcohols, including methanol, ethanol and 1-propanol [7]. The functional groups were too small to effectively change the mean pore diameter, tortuosity, porosity or surface area. However, single gas permeation experiments demonstrated an increase in surface flow for gases without permanent dipole moments (CO_2, C_3H_8 and R-114), and a decrease in surface flow for a polar gas (R-22). Although improvement in selectivity was modest, there was a notable increase in the effective diffusivity of C_3H_8 corresponding to an increase in carbon number of the functional groups.

Miller and Koros modified γ-alumina ultrafiltration (UF) membranes with a 4 nm pore diameter using tridecafluoro-1,1,2,2,-tetrahydrooctyl-1-trichlorosilane [8]. The pore size of the UF membrane was reduced to separate low molecular weight liquids, such as solvents from lube oils. Single gas permeation experiments indicated a decrease in permeability of up to 2 orders of magnitude, and a small decrease in selectivity of He over Ar and SF_6 compared to the unmodified membrane. However, the reduction in pore size was not sufficient to prevent the flow of lube oil.

Castro et al. grafted polyvinylpyrrolidone chains onto silica supports with starting pore diameters ranging 0.12 - 0.41 μm [9,10]. They used a two step graft polymerization process where vinyl-alkoxysilanes were used as coupling agents for polyvinylpyrrolidone monomers. The polymer brush-layer increased selectivity without decreasing permeability for the cross-flow filtration of an oil/water emulsion and reduced fouling.

Hyun et al. used phenyltriethoxysilane to modify the surface of γ-alumina UF membranes with an initial pore size of 2.2 nm [11]. The silanization resulted in an order of magnitude decrease in permeance of CO_2 and N_2 and a selectivity for CO_2/N_2 as high as 2.3. The selectivity observed for the heaviest component over the lightest component from a mixture, or *reverse selectivity*, was a significant result. The theoretical Knudsen selectivity, α, calculated as the square root of the ratio of the inverse ratio of the molecular weights of species i and j:

$$\alpha_{i/j} = \sqrt{\frac{M_j}{M_i}} \qquad (2.1)$$

predicts a selectivity for N_2/CO_2 of 1.25. Reverse selectivity is considered a result of selective adsorption and surface flow due interactions between the material and the penetrants [12]. The selectivity was proportional to the concentration of CO_2 in the feed mixture, and the modified membrane was stable up to 100 °C.

Leger et al. grafted polydimethylsiloxane (PDMS) onto γ-alumina membranes with a pore size of 5 nm by thermal decomposition of silicone oil [13]. The membrane proved to be selective for volatile organic compounds (VOCs) over water by pervaporation. Single gas permeation experiments reported a decrease in permeability of about 4 orders of magnitude. The ratio of pure gas permeabilities indicated reverse selectivity for $CO_2/N_2 = 10.2$ and $C_3H_8/N_2 = 13.8$. The interaction of the PDMS with hydrocarbons was further supported by the selectivity of $CH_4/N_2 = 18.3$. The selectivities observed for the PDMS treated alumina were lower than for pure PDMS membranes. However, the composite membrane was chemically stable in pure organic solvents (i.e., toluene) and thermally stable up to 300 °C.

In a subsequent paper, Leger et al. used octadecyltrichlorosilane to modify γ-alumina supports with a pore size of 5 nm for gas separations [14]. The trichlorosilanes reacted with hydroxylated surfaces through a direct substitution reaction that attached the octadecylsilane (ODS) molecules to the surface. Pure gas permeabilities were decreased by 3 orders of magnitude, resulting in reverse selectivity of CH_4/He and CO_2/N_2. They reported the order of permeabilities for the untreated membrane to be He > CH_4 > C_3H_8 > N_2 > CO_2 > Ne > Ar in contrast to the order for the ODS treated membrane CH_4 > He > ($C_3H_8 \cong CO_2$) > N_2 > Ne > Ar. Permeabilities were reduced by a factor of 5 after exposure to a 1 atm N_2 feed with vacuum on the permeate side. They assumed this phenomena was caused by compaction of the ODS layer and permeabilities were recovered in the absence of vacuum after several hours, by reversal of the pressure difference, or after rinsing in toluene.

Mejean et al. used dodecyl-triethoxysilane, $(C_2H_5O)_3SiC_{12}H_{25}$, and tridecafluoro-1,1,2,2-tetrahydro-octyloxypropyl-triethoxysilane, $(C_2H_5O)_3SiO(CH_2)_3C_6F_{13}$, separately to modify γ-alumina membranes with a pore size of 5 nm [15]. Single gas permeability tests for the membrane functionalized with dodecyl-triethoxysilane agreed with the experiments by Leger et al. except that their membrane was selective for CO_2 and C_3H_8 over He. Selectivities ranged from 2 to 4 for C_3H_8 and CO_2 over N_2 and He for feed pressures between 17.6 and 51.4 psia. The membrane modified with the fluorinated functional group showed a sharp decrease in the permeability of hydrocarbons, with increased selectivities for CO_2 over C_3H_8 and N_2 of approximately 2.5-3.5. The order of permeability was $C_3H_8 > CO_2 > He > N_2$ for the dodecyl-triethoxysilane functional group and $CO_2 > He > C_3H_8 > N_2$ for the fluorinated group.

In this chapter we investigate the use of ODS to modify commercially available porous membranes for gas separations. Countless silane coupling agents exist commercially or can be synthesized, however octadecyltrichlorosilane is the most popular compound for coupling long chain hydrocarbons to inorganic surfaces. We discuss selectivity of the ODS membrane and a phenomenological model of pure gas transport for various light and condensable gases. We also investigate the surface chemistry of the ODS layer by using modified surrogate porous alumina and dense polycrystalline sapphire samples.

2.2 Theory

Pure gas permeation provides a baseline for the comparison of membrane performance and an indication of the mechanisms of transport that control the permeation of various gases. Transport models in this chapter are based on a surface diffusion enhanced micropore permeation (SEMP) model, developed by Burggraaf, who used the model to predict flux though silicalite membranes using known properties of zeolites[16,17]. Although the permeation behavior of the ODS membrane performs similar to other microporous membranes, such as zeolite films, it does not fit into the same class of materials. Because of this, we simplified the model to neglect information about microstructure of the membrane, and we refer it as the surface diffusion enhanced permeation (SEP) model. In this chapter, we examine the fit of the SEP model to experimental pure gas permeation data to gain understanding of transport through the membrane. The model has been derived to investigate transport based on surface diffusion in the presence of Langmuir adsorption, for condensable gases, and adsorption in the Henry regime, for lighter gases.

2.2.1 *SEP Model with Langmuir Adsorption*

Although the Langmuir isotherm is theoretically simple, it fits a great number of experimental isotherms for microporous and dense materials reasonably well [18,19]. The Langmuir isotherm for the adsorption of a single gas is given as:

$$\theta = \frac{q}{q_s} = \frac{K\,p}{1 + K\,p} \tag{2.2}$$

where θ is the occupancy, q is the amount adsorbed of gas adsorbed per unit sorbent, q_s is the amount adsorbed at saturation, p is pressure and K is the Langmuir sorption constant. The expression for gas flux (J) through a membrane under isothermal conditions is:

$$J = -\mu^* D_c(q)\Gamma \frac{\mathrm{d}q}{\mathrm{d}z} \tag{2.3}$$

where $D_c(q)$ is the intrinsic diffusion coefficient, μ^* is a geometric factor related to the porosity and Γ is the thermodynamic factor [17]. The Fickian diffusion coefficient (D_F) is equal to $D_c(q)\ \Gamma$ and is assumed to be constant. Equation (2.3) can be integrated over the thickness (L) of the membrane to derive an explicit expression for flux:

$$J = \frac{\mu^* q_{\mathrm{sat}}}{L} D_F \ln\left(\frac{1 + Kp_f}{1 + Kp_p}\right) \tag{2.4}$$

where p_f and p_p, are pressures in the feed and permeate streams, respectively. Equations (2.3) and (2.4) are in agreement with the generalized Stefan-Maxwell theory reduced for single gases, in which the driving force is considered to be the gradient in the concentration of the surface adsorbed species [20]. Temperature dependence is introduced into the model by substituting the Arrhenius relation for D_F and K:

$$D_F = D_{F,o} exp\left(\frac{-E_d}{RT}\right) \tag{2.5a}$$

$$K = K_o \exp\left(\frac{Q_a}{RT}\right) \tag{2.5b}$$

where Q_a is the isosteric energy of adsorption and E_d is the intrinsic activation energy of diffusion. The SEP model does not account for bulk flow that would be expected if larger pores exist and it was assumed that D_F is not a function of the gas concentration in the porous material [17].

2.2.2 *SEP Model in the Henry Adsorption Regime*

Sorption of non-condensable gases, such as H_2 and N_2, typically occurs in the *Henry adsorption regime* where the occupancy of sorption sites on the surface of membrane is low and is known to be linear with pressure, usually at high temperature and/or low pressure. At low surface concentrations $K p << 1$, and equation (2.2) reduces to the linear relation:

$$q = K q_s p \tag{2.6}$$

Equation (2.4) describing the flux of gases in the Langmuir regime can be simplified to obtain the flux for the Henry regime:

$$J = \frac{\mu^* D_{F,o} q_s K_o}{L} \exp\left(\frac{(Q_a - E_d)}{RT}\right)(p_f - p_p) \tag{2.7}$$

All pre-exponential parameters, except for K_o, in equation (2.4) and (2.7) were lumped into one term for mathematical convenience, as given below:

$$A = \frac{\mu^* D_{F,o} q_{sat}}{L} \tag{2.8}$$

The SEP model for the Langmuir regime, equation (2.4), and Henry regime, equation (2.7), show the relationship between Q_a and E_d. However these parameters cannot be uncoupled unless transport experiments are performed at high temperatures where adsorption is eliminated. The effects of adsorption and surface flow in microporous materials has been observed at temperatures above 473 K [16,17,21-23], which is beyond range of temperatures studied for this membrane. Silane layers are reported to be stable at temperatures between 373 K and 500 K [11,24]. It is common to report the *apparent activation energy* (E^+) as given below:

$$E^{+} = Q_a - E_d \tag{2.9}$$

The value of E^+ can be determined from a fit of a transport model, such as the SEP model, to permeation data determined over a range of temperatures.

2.3 Experimental

2.3.1 *Silanization*

Asymmetric alumina ultrafilters (U.S. Filter T-170, Warrendale, PA) with a mesoporous top layer were modified using octadecyltrichlorosilane. Figure 2-1 shows the cross section view of the inside bore of an unmodified U.S. Filter ultrafilter. The γ-alumina barrier layer deposited on the inside surface of the tube has a nominal 5 nm pore size and is approximately 5 μm thick. The tube was cut into 5.4 cm sections and lead-silicate glaze (Duncan GL 612, Fresno, CA) was used to seal the ends prior to silanization.

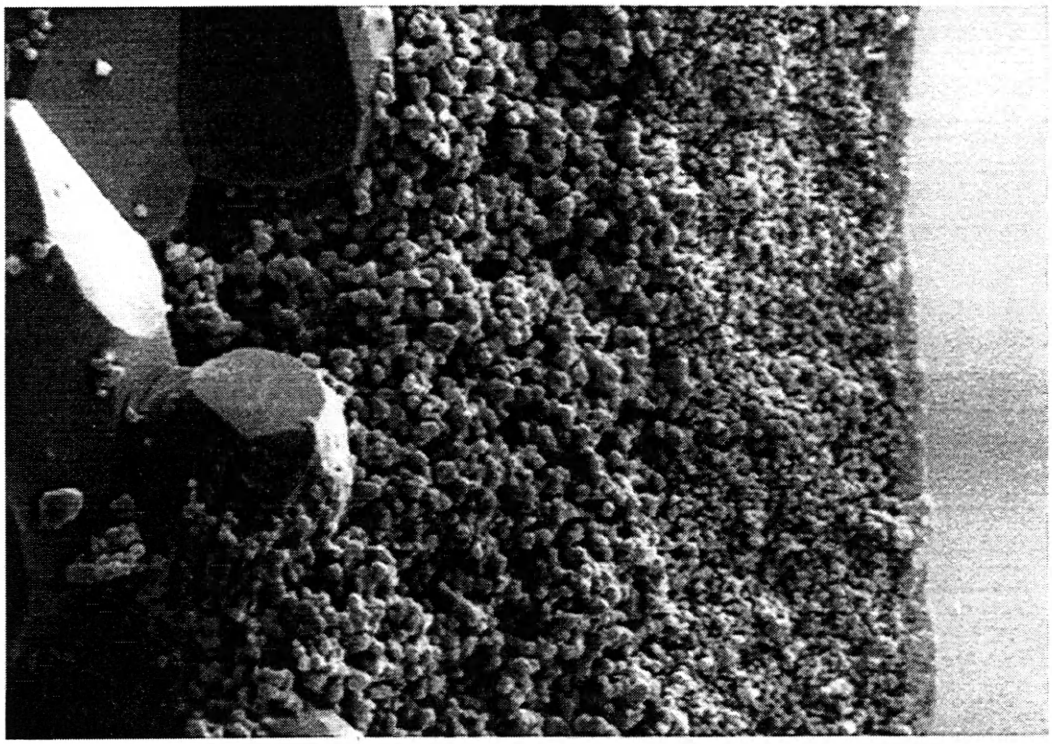

Figure 2-1: A scanning electron micrograph of a U.S. Filter T-170 alumina ultrafilter. This is a cross section view looking down the inside bore of the tube. The γ-alumina top layer indicated by the white arrows is approximately 5 μm thick.

The silanization process used was similar to the technique used by Leger et al. [14] and can be divided into the four steps outlined below:

1) Sample Preparation
   a) Clean the unmodified sample by heating at 10 °C/minute to 400 °C in air.
   b) Boil sample in 30% hydrogen peroxide for 30 minutes.
   c) Boil sample in distilled water for 30 minutes to hydroxylate the surface.
   d) Dry sample for 30 minutes at 90 °C.

2) Silanization
   a) Place the sample and 120 ml of HPLC grade toluene into a triple-neck flask.
   b) Transfer 5 ml of the octadecyltrichlorosilane (United Chemical Technologies, Inc., Bristol, PA) and 10 ml HPLC grade toluene into a graduated cylinder and seal. This is performed inside a glove bag under flowing nitrogen and seal to avoid reaction with atmospheric water.
   c) Add the octadecyltrichlorosilane/toluene mixture into the triple-neck flask and rinse the neck of the flask with an additional 10 ml of toluene.
   d) Reflux for approximately 3 hours at 400 Torr and room temperature.

3) Rinsing
   a) Place sample into funnel with silica-frit and rinse with approximately 1 L of HPLC grade toluene.
   b) Place in 400 ml toluene and soak for approximately 12 hours.

4) Drying
   a) Dry for at least 12 hours at 65 °C.

Each step has a significant effect on the morphology of the ODS layer. In particular, the sample preparation and silanization steps deserve extensive study in the future. Sample preparation determines the density of hydroxyl groups and physically adsorbed water on the surface prior to silanization. Varying temperature, solvent type and silane concentration during silanization affects thickness and roughness of the deposited layer.

2.3.2 *Surface Analysis*

Surface analysis using transmission Fourier transform infrared spectroscopy (FTIR), variable angle spectroscopic ellipsometry (VASE) and x-ray photoelectron spectroscopy (XPS) was performed to characterize the ODS layer deposited onto the surface of the mesoporous substrates. This analysis was performed on surrogate samples instead of the membrane to provide an ideal surface for these experiments. Although deposition often varies between surfaces, this approach provided evidence and a baseline for comparison to understand the nature of the ODS layer grafted onto the porous alumina.

The surrogates included a flat, dense, polycrystalline sapphire disk and a 0.2 μm Anodisc alumina filter (Whatman, Inc.; Hillsboro, Oregon) that that were modified in the same vessel as the U.S. Filter tube throughout the silanization and rinsing processes. The sapphire samples were rinsed with toluene, placed with the silane-layer side down on a covered watch glass and stored in a dessicator prior to analysis. The samples were also rinsed with toluene within 10 minutes prior to surface analysis experiments.

2.3.2.1 *FTIR Spectroscopy*

Transmission FTIR was performed using a Biorad (Cambridge, MA) FTS 40 FTIR to confirm the presence of the silane on the surface of a surrogate sample. An Anodisc was cleaned by boiling in 30% hydrogen peroxide for 30 minutes, rinsing with distilled water for about 30 minutes and dried at 90 °C before being mounted for transmission FTIR analysis 'as received'. Subsequently, the same Anodisc sample was treated with octadecyltrichlorosilane following the procedures described above, along with the tubular sample, and transmission FTIR analysis was repeated.

2.3.2.2 *Ellipsometry Measurements*

The thickness of the ODS layer deposited on a flat polycrystalline sapphire sample was measured using a variable angle spectroscopic ellipsometer (VASE®; J.A. Woollam Co., Inc., Lincoln, NE). One side of the sapphire disk was roughened by blasting with alumina sand to diffuse light and eliminate the signal from the backside of the sample. Spectra were generated at angles of 60°, 65° and 70° with wavelengths ranging from 300 to 900 nm before and after silanization. The unmodified substrate was optically clear and the measured values for the index of refraction were in agreement with the literature from the WVASE32 library [25,26]. Subsequently, spectra were generated for the octadecyltrichlorosilane modified sample under the same conditions. The ODS layer was assumed to be optically clear with a refractive index of 1.45 as reported by Wasserman et al. [27].

2.3.2.3 *X-Ray Photoelectron Spectroscopy (XPS)*

The XPS spectra were taken on the ODS layer deposited on sapphire using a Kratos HSi (Shimadzu Scientific Instruments, Inc.,Columbia, Maryland) spectrometer referenced to C_{1s}. The X-ray source was operated at 15 mA and 14 kV. The residual pressure in the spectrometer chamber during data acquisition was less than 5×10^{-10} Torr. Take-off angles relative to the sample surface were fixed at 90° and 30° to obtain scans that were more bulk sensitive and surface sensitive respectively.

2.3.3 *Transport Measurements*

Pure gas fluxes were measured for membranes before and after modification using a steady-state permeance method during which the feed and permeate pressures were set and the permeate flow rates were measured [22]. Feed and permeate pressures were set using backpressure regulators and the permeate flow rates were measured using bubble flow meters. Cross flow feed was maintained through the bore of the tubular sample using mass flow controllers ranging from 10 to 20 scc/minute, except when the flow rates were extremely high (before silanization) and dead-end fluxes were measured.

The samples were mounted with Viton o-rings into a stainless steel shell and tube flow cell (Figure 2-2) that was placed in a thermostatic water bath. The He, H_2 and N_2 used for transport experiments were 99.999% pure (General Air, Denver, CO). The CO_2, CH_4 and C_2H_6 (General Air, Denver, CO) and n-C_4H_{10} and i-C_4H_{10} (Scott Specialty Gases, Longmont, CO) were at least 99.0% pure. The gases were used without further purification.

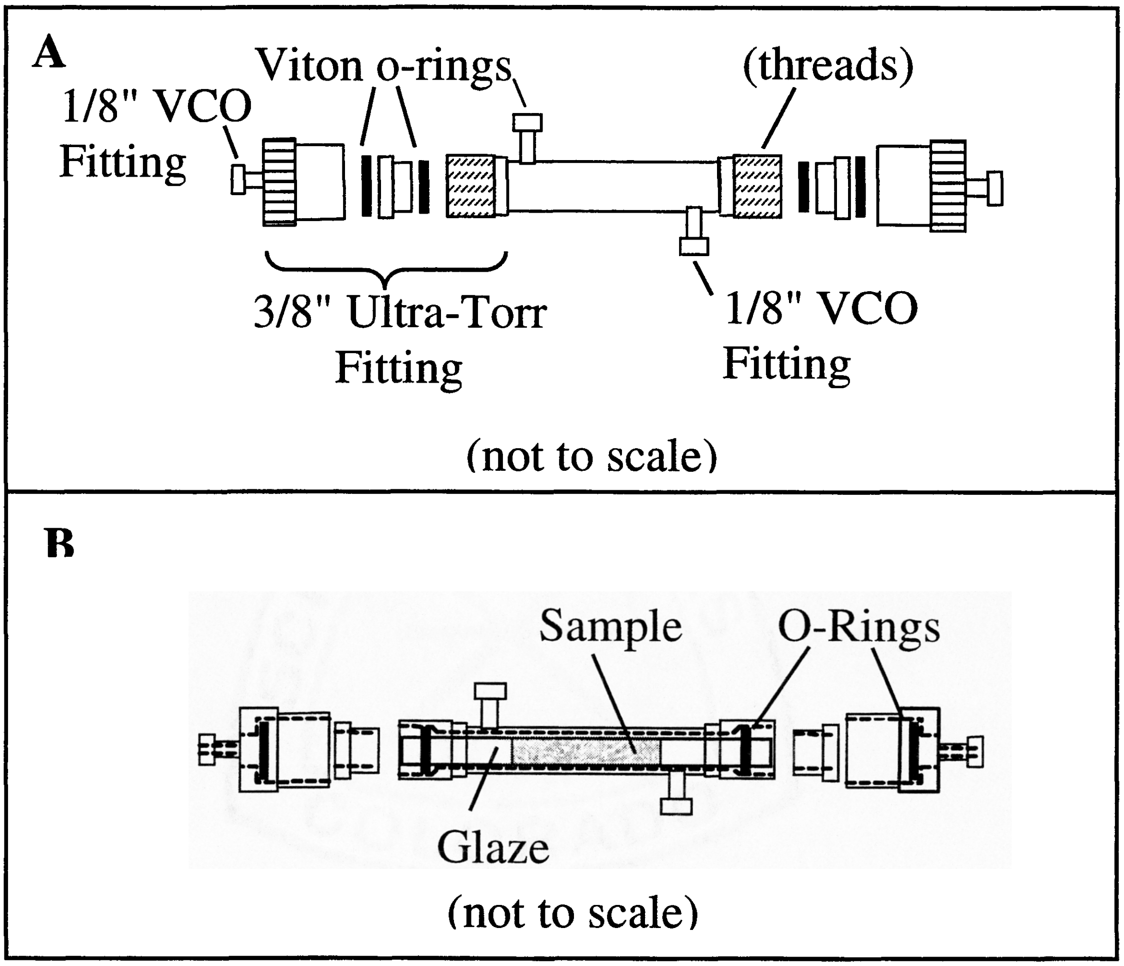

Figure 2-2: Schematics of the stainless steel cross-flow membrane module for 2 inch tubular samples; A) describing the construction of the module, B) describing the assembly of the module with a membrane.

Mixed gas separations were performed using the same apparatus as the pure gas experiments, however the permeate and residue streams were routed to a gas chromatograph (GC) to determine the composition [22]. For separation experiments performed without permeate sweep gas, the pressure driving force was calculated assuming a linear concentration (partial pressure) profile on the feed side (through the bore of the tube), as shown below:

$$P_i = -\frac{J_i}{\Delta p_i} = \frac{J_i}{1/2\left(p_i^f + p_i^r\right) - p_i^p} \tag{2.10}$$

where P was the permeance, J was the flux and p was the partial pressure of component i. Superscripts f, r and p designate the feed, residue and permeate streams, respectively.

A log mean driving force $\left(\Delta p_i\right)_{lm}$ was assumed for experiments using a He sweep gas in the permeate stream:

$$P_i = -\frac{J_i}{\left(\Delta p_i\right)_{lm}} \tag{2.11}$$

where $\left(\Delta p_i\right)_{lm}$ was defined as:

$$\left(\Delta p_i\right)_{lm} = \left\{ \frac{\left(p_{i,2}^f - p_{i,2}^p\right) - \left(p_{i,1}^f - p_{i,1}^p\right)}{\ln\left(\dfrac{p_{i,2}^f - p_{i,2}^p}{p_{i,1}^f - p_{i,1}^p}\right)} \right\} \tag{2.12}$$

and subscripts 1 and 2 designate inlet and outlet ends of the tube, respectively.

Selectivity for pure gases and mixed gas separations was defined as the ratio of the gas permeances:

$$\alpha_{i/j} = \frac{P_i}{P_j} \tag{2.13}$$

A Hewlett Packard 5890 series II GC with thermal conductivity detector (TCD) and flame ionization detector (FID) was automated using Hewlett Packard ChemStation software to perform the analysis. A ten port Valco valve was used to sample permeate and residue streams during separations experiments. A 600 cm long Alltech Haysep-Q packed column with helium sweep gas was used with a temperature ramp between 323 K and 473 K to obtain baseline to baseline separation of all components.

2.4 Results and Discussion

2.4.1 *Pure Gas Transport through the Substrate Prior to Silanization*

Pure gas permeance and selectivity were used to gauge the integrity of the 5 nm alumina membrane (U.S. Filter, T-170) and to set a baseline for the sample's performance prior to silanization. Table 2-1 lists the selectivities of several penetrants, as well as the theoretical Knudsen selectivities calculated using equation (2.1). Permeance was measured at 293 K, with a feed pressure of 10.0 psig and a permeate pressure of 5.0 psig. Knudsen selectivity is expected when the mean pore diameter of the membrane is much less than the mean free path of the gas, and other transport mechanisms such as viscous flow and molecular diffusion do not contribute significantly. The mean free path for the gases studied range from approximately 35-130 nm, or 7 to 26 times the mean pore diameter, for $i\text{-}C_4H_{10}$ and H_2 respectively.

Table 2-1: A comparison of the pure gas selectivity for unmodified U.S. Filter T-170 5nm with theoretical Knudsen selectivities.

Penetrants	Theoretical Knudsen Selectivity	Pure Gas Selectivity
H_2/He	1.41	1.41
H_2/N_2	3.74	3.41
$i\text{-}C_4H_{10}/H_2$	0.186	0.643
$i\text{-}C_4H_{10}/N_2$	0.695	2.20

The H_2/N_2 selectivity of 3.41 is 8.8% lower than the theoretical Knudsen selectivity of 3.74. The decrease in selectivity may be due to surface flow of N_2. Nitrogen is known to interact with hydroxyl groups on inorganic surfaces, which is one factor can increase transport through the alumina supports by surface flow [21].

The reverse selectivity observed for $i\text{-}C_4H_{10}/N_2$ is further evidence that permeance is enhanced by surface flow. The theoretical Knudsen selectivity predicts that the lightest components would diffuse fastest, hence the Knudsen selectivities for $i\text{-}C_4H_{10}$ over the N_2 and H_2 listed in Table 2-1 are less than one. The support is not selective for $i\text{-}C_4H_{10}$ over

H_2, however the i-C_4H_{10}/H_2 selectivity is 3.5 times higher than the calculated Knudsen selectivity. Surface flow enhanced permeabilities for heavier gases, including Ar and SF_6 compared to He, were observed for the same material by Miller and Koros [8].

A plot of the pure gas permeance as a function of the *mean trans-membrane pressure*, the average of the feed and permeate pressures, is shown in Figure 2-3. Linear pressure dependence with an insignificant slope is typical of flow that is predominantly Knudsen diffusion [16]. For viscous flow, flux has a second order dependence on pressure, or permeance has a linear dependence on mean trans-membrane pressure with a positive slope [16]. In this case, a significant positive slope would be considered evidence of viscous flow due to defects in the γ-alumina top layer, or in the lead-silicate glaze that seals the ends of the tube. The fact that Knudsen flow and surface flow are the dominant transport mechanisms, and reverse selectivity is observed for the unmodified substrate suggests that this is a reasonable starting material for the development of a gas separation membrane.

2.4.2 *Surface Analysis*

A comparison of the transmission-FTIR spectra for the Anodisc before and after modification with octadecyltrichlorosilane, shown in Figure 2-4, confirms the presence of the ODS layer. The sharp methyl stretches seen between 2850 and 3000 cm^{-1} indicate the hindered motion of alkylsilanes coupled with the surface. Ellipsometry measurements indicate that the thickness of the silane layer deposited on a sapphire wafer is

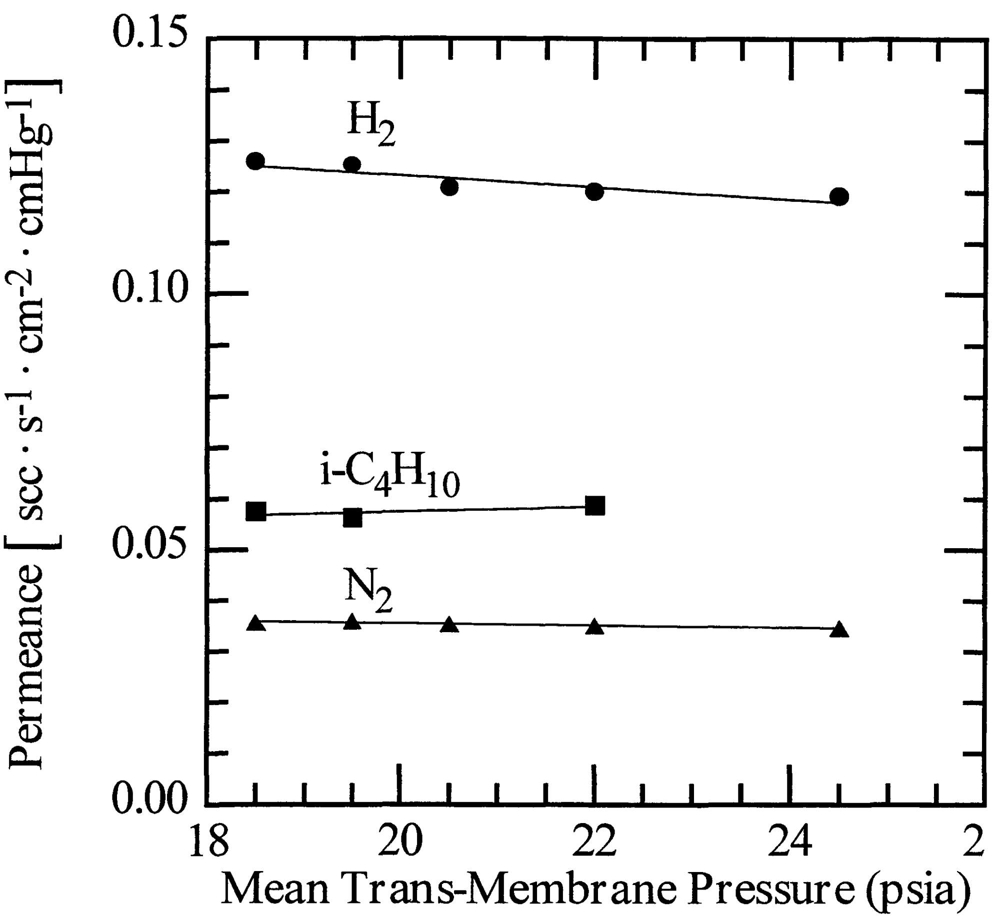

Figure 2-3: Pure gas permeance as a function of mean trans-membrane pressure for a 5.0 nm U.S. Filter T-170 membrane prior to modification.

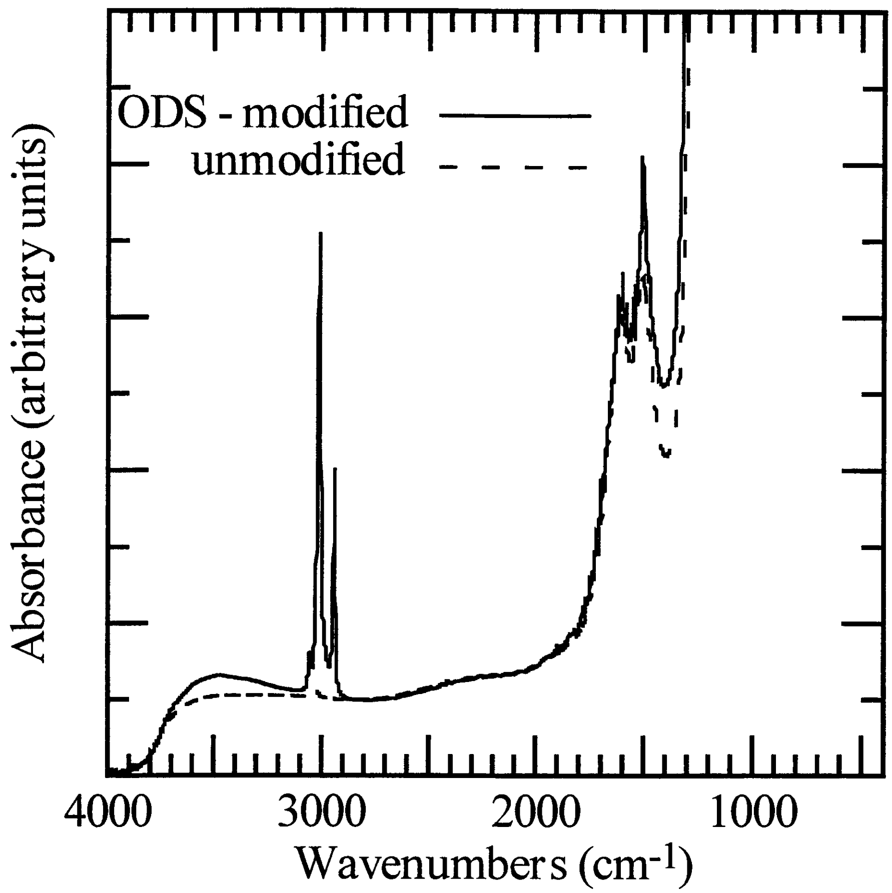

Figure 2-4: Transmission FTIR spectra for a 0.2 μm Anodisc before and after modification with ODS. The sharp methyl stretches seen between 2850 and 3200 cm^{-1} indicate the hindered motion of alkyl-silanes grafted on the surface.

approximately 10.1 nm, which is approximately 7.6 nm larger than a monolayer thickness of 2.5 nm [27]. Covalent linking of at least five layers, or a polymerized layer bonded to the surface would be required to achieve a layer of this thickness [3,27-29].

The XPS analysis of the ODS layer deposited on a surrogate sapphire disk identified different species of silicon associated with a bulk layer and an interface at the sapphire surface. There was no chlorine detected indicating that all of the trichlorosilanes had reacted, and there was no shift associated with carbon. The Si2p spectra at 102.1 eV associated with the interface was distinguished from Si2p at 103.3 eV in a bulk layer, by observing an increase in the respective peak areas when the take off angle relative to the sample surface was decreased from 90° to 30°. A core level shift relative to oxidation state observed by Hollinger et al. [30] was consistent with the 1.2 eV shift observed between the sapphire interface and a bulk layer that was in a less ionic valence state.

The original premise of our experiment was that silanization would result in a self-assembled monolayer with the relaxed ODS chains extending away from the surface. However, even under ideal conditions the deposition of a monolayer (composed of close-packed, trans-extended, vertical chains) is difficult and often irreproducible [31]. Problems in ODS layers reported in literature, included variations in density, cross-linking between adjacent alkylsilane molecules (-Si-O-Si-), and polymeric phases [2,3,31,32]. The thickness of the ODS layer measured by ellipsometry was approximately 5 times greater than a monolayer thickness. In addition, XPS analysis supports these observations by identifying two species of silicon associated with a bulk layer and an interface. If a monolayer had been deposited then only the spectra for silicon at the interface would be observed. The morphology of the ODS layer on the porous substrate is still not well defined, therefore the polymer film may have been deposited inside of the pores, or as a thin film covering the porous alumina surface. In light of these observations our hypothesis changed, and the composite membrane was believed to be composed of a very thin selective polymer film of ODS molecules interconnected with the porous alumina surface.

2.4.3 *Pure Gas Permeance of the ODS Membrane*

A summary of selectivities, or ratios of permeances, measured with pure gas permeation experiments for the ODS membrane is included in Table 2-2. The pure gas permeances were measured at 293 K with a feed pressure of approximately 22.0 psia and permeate pressure of 17.0 psia. The permeances of the ODS membrane were observed to be history dependent, with increases from the initial N_2 permeance as high as 30% and decreases of 71% noted over a 16-month period. Permeances were recovered to within ±10 % of their original value by rinsing the membrane in toluene and drying at 233 K, or by exposure to flowing nitrogen under a small pressure drop (5.0 psi) for 24 hours. This phenomena was consistent with results of Leger et al. [14] who observed variations in permeability of an ODS layer after exposure to vacuum. To eliminate variability between pure gas selectivities, the pure gas permeance data were taken during a period of one day.

Table 2-2: Summary of pure gas selectivities for an ODS membrane.

Mixtures	Theoretical Knudsen Selectivity	Pure Gas Selectivity
n-C_4H_{10}/H_2	0.186	14.4
n-C_4H_{10}/N_2	0.695	48.2
n-C_4H_{10}/CO_2	0.871	9.4
n-C_4H_{10}/CH_4	0.525	19.6
n-C_4H_{10}/C_2H_6	0.719	7.0
n-C_4H_{10}/i-C_4H_{10}	1.00	1.6
CO_2/N_2	0.871	5.1
CO_2/CH_4	0.603	2.1
H_2/CH_4	2.82	1.4

Reverse selectivity was observed for all condensable species (gases below critical temperature) including n-C_4H_{10}, i-C_4H_{10}, CO_2 and C_2H_6. Note that the theoretical Knudsen selectivity is less than one for cases when the membrane displayed reverse selectivity. The order of selectivity (n-C_4H_{10} > i-C_4H_{10} > C_2H_6 > CO_2 > H_2 > CH_4 > N_2) was consistent with the results by Mejean et al. [15], who observed reverse selectivity for higher hydrocarbons and CO_2 over CH_4. In addition, we observed significant selectivities for butanes and CO_2 over H_2, CH_4 and N_2.

Pure gas permeances of the ODS membrane are presented in Figure 2-5 plotted against critical temperature. Since solubility is an exponential function of temperature, this plot shows the relationship between the permeance and solubility of these gases with this membrane that indicates transport was strongly influenced by preferential adsorption [33,34]. The permeance of H_2 does not fit the exponential relationship with critical temperature, therefore adsorption of H_2 was less significant.

2.4.4 *Mixed Gas Separations*

Mixed gas separation experiments were designed to measure selectivities that occur in an environment where competitive adsorption and significant surface flow exist. Mixed gas selectivities measured using cocurrent flow, with and without a He sweep gas, are presented in Table 2-3. Feed and permeate pressures were maintained at approximately 32.0 psia and 17.0 psia, respectively, and temperature was controlled at a constant 293 K. Feed mixtures containing 20 ±2% of the more strongly adsorbing species (either n-C_4H_{10} or CO_2) were delivered either by a premixed gas, or with gas mixed with mass two flow controllers. Nitrogen flux was checked between mixed gas experiments to maintain consistency. If N_2 flux was not within 10% of the original value the membrane was cleaned as described in Section 2.4.3.

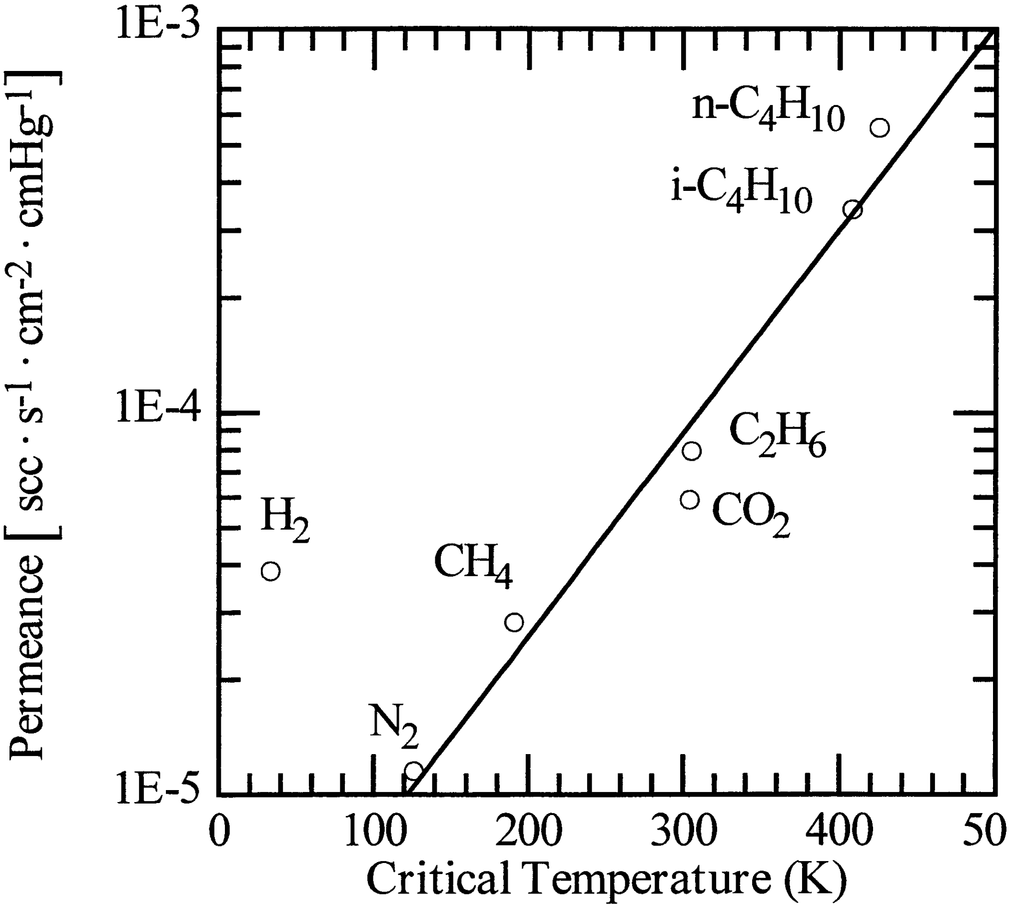

Figure 2-5: Pure gas permeance through the ODS membrane follows an exponential relationship with critical temperature. This is an indication that transport is controlled by preferential adsorption.

Table 2-3: Summary of mixed gas selectivities observed for the ODS membrane.

Mixtures	Mixed Gas Selectivity w/ He Sweep	Mixed Gas Selectivity No Sweep
$n\text{-}C_4H_{10}/H_2$	4.3	11.1
$n\text{-}C_4H_{10}/N_2$	10.8	42.8[a]
$n\text{-}C_4H_{10}/CO_2$	n/a	10.7[a]
$n\text{-}C_4H_{10}/CH_4$	7.0	24.0
$n\text{-}C_4H_{10}/C_2H_6$	3.4	10.8
CO_2/N_2	n/a	5.8[b]
CO_2/CH_4	n/a	4.3
H_2/CH_4	n/a	2.2

a. Upper limit of selectivity estimated using equation (2.10) while setting $p^P_{n-C_4H_{10}} = p^R_{n-C_4H_{10}}$.

b. Feed mixture: 48.7% N_2 and 51.3% CO_2.

The use of a He sweep gas, or carrier gas, in the permeate stream reduced selectivity significantly. We believe this was a consequence of a reduction of adsorbed n-C_4H_{10} in the membrane, attributed to the back diffusion of He. Due to these observations, most of the separations were performed without a sweep and further discussions will be limited to experiments performed without a sweep gas.

During n-C_4H_{10}/N_2 and n-C_4H_{10}/CO_2 separations (cocurrent flow without sweep gas), it was found that transport of n-C_4H_{10} was limited by the available concentration (partial pressure) driving force. In other words, the flux of n-C_4H_{10} was so high, compared to the membrane area and feed flow rate, that $p^R_{n-C_4H_{10}}$ and $p^P_{n-C_4H_{10}}$ became equal within the resolution of the GC. Although this is not intuitive, Appendix 2 presents a model that shows this is a reasonable result. This transport limitation could artificially depress mixed gas selectivities. By applying the model in Appendix 2 using pure gas permeances, the mixed gas separations experiments (cocurrent flow without sweep gas) can be designed to avoid driving force limitations and depressed selectivities.

The mixed gas selectivities for n-C_4H_{10} over CH_4 and C_2H_6 were 14.8% and 54.3% higher than the pure gas selectivities, respectively, indicating enhanced selectivity in a mixture due to competitive adsorption [12,21,22]. Competitive adsorption refers to a phenomenon where more strongly adsorbing gases block access to adsorption from other gases in mixture (see Appendix 1). Further evidence of competitive adsorption was a 10% increase in selectivity of CO_2/CH_4, while the CO_2/N_2 selectivity more than doubled for the mixed gas experiments over pure gas selectivities.

Rao and Sircar [12] observed reverse selectivity through competitive adsorption with nanoporous carbon membranes, which correlated to a relative reduction in permeance for the gases that were blocked. Although the same correlation was not observed for the ODS membrane, there was a relative change in permeance with selectivity. Table 2-4 is a summary of the permeances used to calculate the selectivities of the pure gas and mixed gas experiments shown in Tables 2-2 and 2-3. The ratios of the permeances for each mixture are presented for easy comparison with their respective selectivities. The change in permeance observed relative to the increase in selectivity of mixed gases for n-C_4H_{10} from CO_2 and N_2 are not a good examples, because of the observed driving force limitations.

During the mixed gas separation of n-C_4H_{10}/C_2H_6 the permeance of C_2H_6 decreased by 29% and the permeance of n-C_4H_{10} increased by 10% relative to the pure gas values, which was consistent with an increase in selectivity due to competitive adsorption of n-C_4H_{10}. With mixed gas separation of n-C_4H_{10}/CH_4 the permeances of both n-C_4H_{10} and CH_4 were about 26% and 39% lower than their pure gas permeances, respectively, however the relative decrease in permeance was greater for CH_4, which also considered a result of competitive adsorption.

The decrease in mixed gas selectivity for n-C_4H_{10}/H_2 compared to the pure gas selectivities was attributed to the mobility of H_2 due to its molecular weight and size. Also, as shown in Figure 2-5, the diffusion of H_2 does not show dependence sorption, therefore competitive adsorption has a less significant effect on selectivity.

Table 2-4: Summary of pure and mixed gas permeances for mixtures studied with the ODS membrane. All permeances are given in cgs units $(scc \cdot s^{-1} \cdot cm^{-2} \cdot cmHg^{-1}) \times 10^{-4}$.

Mixtures	**Ratio of Pure Gas Permeances**	**Ratio of Mixed Gas Permeances**
$n\text{-}C_4H_{10}/H_2$	5.54 / 0.385	6.09 / 0.551
$n\text{-}C_4H_{10}/N_2$	5.54 / 0.115	9.11 / 0.213 [a]
$n\text{-}C_4H_{10}/CO_2$	5.54 / 0.591	7.36 / 0.688 [a]
$n\text{-}C_4H_{10}/ CH_4$	5.54 / 0.282	4.12 / 0.172
$n\text{-}C_4H_{10}/C_2H_6$	5.54 / 0.793	6.05 / 0.562
CO_2/N_2	0.591 / 0.115	1.18 / 0.202
CO_2/CH_4	0.591 / 0.282	0.405 / 0.094
H_2/CH_4	0.385 / 0.282	0.210/ 0.097

a. Upper limit of selectivity estimated using equation (2.10) while setting $p^{P}_{n-C_4H_{10}} = p^{R}_{n-C_4H_{10}}$.

The increases in CO_2 selectivity over N_2 and CH_4 for mixed gas experiments followed an increase in the permeance of all gases. However the relative increase in permeance was greater for CO_2 in both cases. It was clear, by the plot of pure gas permeance versus critical temperature and by the increase in selectivity for mixed gases over pure gases, that sorption played a significant role in the permeance and selectivity of the ODS membrane. Also, the correlation between a relative change in permeance with selectivity indicated competitive adsorption occurred. However, there was no correlation in the absolute change in magnitude of the permeances as observed by Rao and Sircar [12]. The variations in permeance were considered to be affected by phase changes in the ODS layer in the presence of mixtures, as well as the diffusivity and solubility of the penetrants.

2.4.5 *Modeling Pure Gas Permeation with Surface Flow*

The initial goal in the development of silane modified membranes was to change the chemical environment within in the porous material to promote adsorption of specific gases and surface flow. Upon examination of the temperature and pressure dependence of gas transport through the ODS membrane, it was immediately recognized that the transport was mechanistically related to phenomena observed with pure gas permeation through microporous zeolite membranes [16,23,35]. We observed a maximum in the permeance of n-C_4H_{10} as a function of temperature and pressure, and the permeance of light gases was found to increase with temperature.

Although the SEP model was developed for flow through microporous materials as opposed to dense polymers, it has also been postulated that in many cases transport through the voids (free volume) in polymer materials is mechanistically similar to transport through microporous materials. This comparison includes materials that exhibit a broad range of crystallinity in which transport takes place within well-defined porous structures and within the free volume of a polymer matrix. Though all of these materials are chemically and morphologically different, gas transport is mechanistically similar and is controlled by sorption and configurational effects.

To study the transport through the ODS membrane we used JMP statistical software [36] to fit the SEP models described in equations (2.4) and (2.7) to pure gas permeance as a function of temperature. Subsequently, we used the parameters from that fit with the same model to predict permeance as a function of pressure. Values for Q_a, E_d, K_o and A were not available in literature for ODS, because transport through this material has not been widely studied for membrane separations. The values of these parameters were arbitrary when the fit converged; however, as long as they were reasonable, or close to literature values for microporous materials [17,23,37], it was found that the value of the apparent activation energy ($E_a = Q_a - E_d$) was constant.

The pure gas permeance for the ODS membrane decreased by approximately two to three orders of magnitude compared to the unmodified sample under the same conditions. As shown in Figure 2-6, the permeance of n-C_4H_{10} as a function of temperature is non-linear and reaches a maximum under these conditions. The maximum

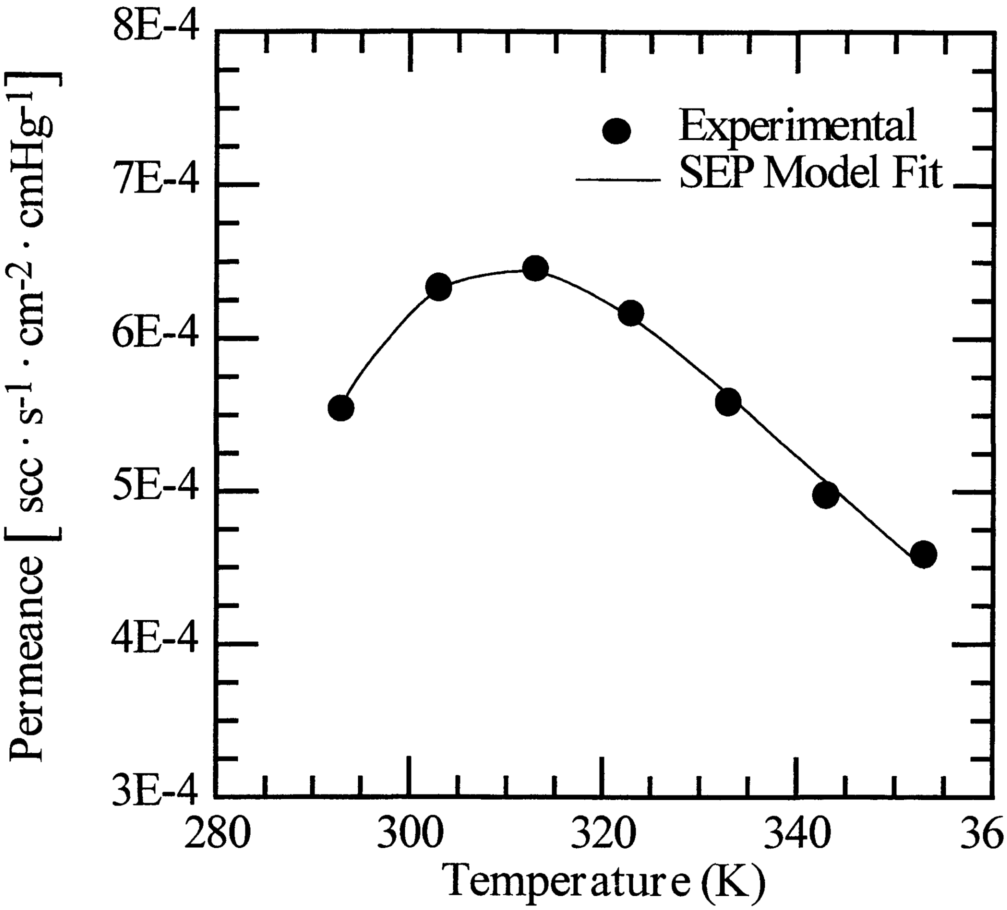

Figure 2-6: The permeance of n-C_4H_{10} as a function of temperature reaches a maximum at approximately 313 K. The SEP model fits the maximum in permeance and estimates E^+ of 2.95 kcal/mole.

permeance occurs at approximately 313 K with an increase of 16.5% over the value measured at 293 K. Beyond that the permeance decreased by 17.3% compared to the value measured at 293 K. The nonlinear fit of the microscopic SEP model, for Langmuir regime adsorption, to the permeance of n-butane as a function of temperature is within a 95% confidence limit with a sum of squared errors of 1.81×10^{-10} ($scc\cdot cm^{-2}\cdot s^{-1}\cdot cmHg^{-1}$).

The SEP model in the Henry regime was used to fit data for light gases including H_2, CO_2 and CH_4 with a 95% confidence level, as shown in Figure 2-7. For the light gases, the sum of squared errors was less than that reported for the more nonlinear fit for n-C_4H_{10}. The SEP model for Langmuir adsorption fit the data for the light gases equally well; however, by fitting the data to the simpler SEP model for Henry adsorption was evidence that these gases are diffusing at low concentrations through the membrane [18,19].

A comparison of the apparent activation energies of diffusion from the SEP fit for the ODS membrane with those reported for silicalite (MFI zeolite), carbon molecular sieve and polyimide membranes is included in Table 2-5. Data given for the silicalite membranes were generated by Kapteyn et al. [38-40] and were used to predict transport through silicalite membrane with the SEMP model by Burggraaf [16]. Both CO_2 and n-C_4H_{10} were shown to be strongly adsorbing ($Q_a > E_d$) on silicalite as indicated by the positive sign for E^+. Studies on polyimide and carbon molecular sieve membranes did not report positive values for E^+.

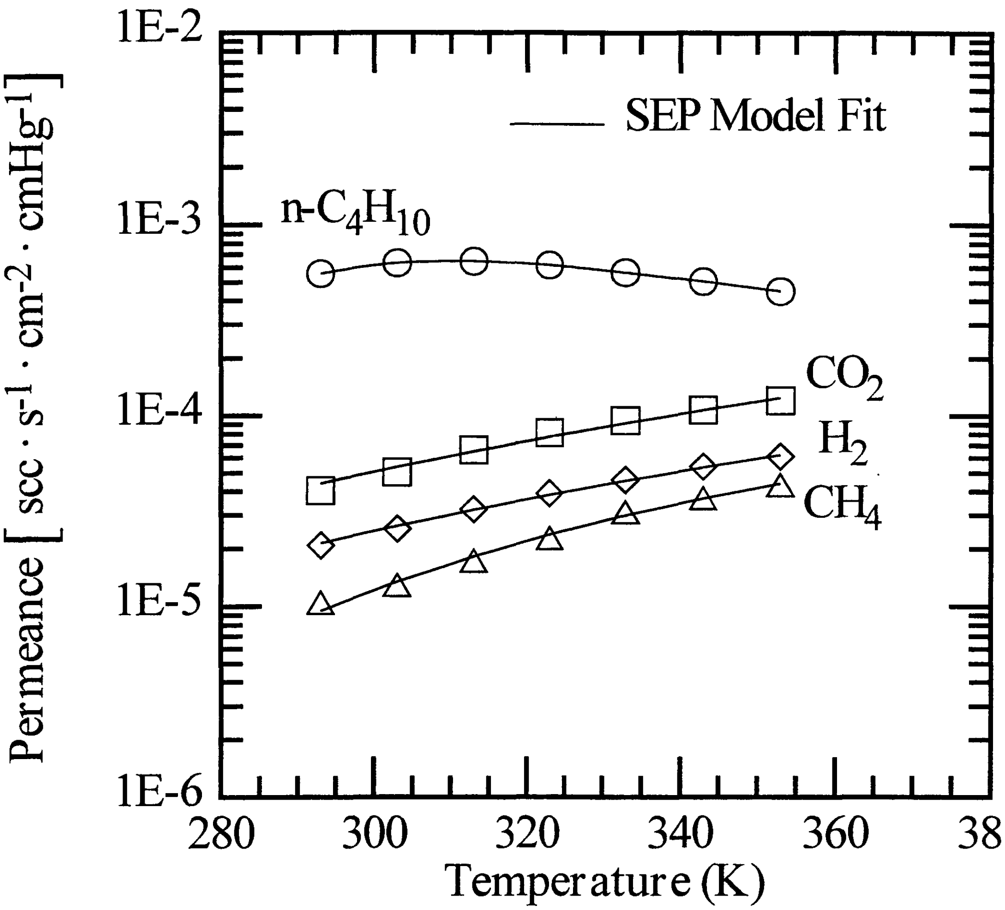

Figure 2-7: A semilog plot of the SEP model fit to permeance as a function of temperature for the ODS membrane. The SEP model fits the transport of n-C_4H_{10} in the Langmuir sorption regime and the lighter gases in the Henry regime.

Table 2-5: Apparent activation energies ($E^+ = Q_a - E_d$) determined for the ODS membrane from the SEP model fit compared to a few values reported in literature for various membranes that exhibit surface flow.

Pure Gas	ODS Membranes E^+ (kcal/mole)	Silicalite Membranes E^+ (kcal/mole)	Carbon Membranes E^+ (kcal/mole)	Polyimide Membranes E^+ (kcal/mole)
n-C_4H_{10}	2.95	2.98	N/a	n/a
CH_4	-4.95	-1.43	-2.34 to -4.78	-1.9 to -8.8
CO_2	-3.55	3.10	-2.94to ≈0	-4.9 to 0.3
H_2	-3.66	-4.06	-2.63	-1.1 to -4.5
Refs.	n/a	17	42-45	46

As reported in literature, the transport of butane under our experimental conditions typically occurs as surface flow in parallel with activated diffusion [16,23,35]. In these cases, surface flow increases with temperature until a maximum in permeance is reached. Beyond this point, sorption is diminished to the point where the decrease in surface flow results in a decrease in the total permeance. This phenomenon is understood to occur in systems where surface flow and activated diffusion occur in parallel and the heat of adsorption (Q_a) of the gas is greater than the intrinsic activation energy of diffusion (E_d). In other words, the apparent activation energy ($E_a = Q_a - E_d$) is positive.

The parameters used to fit the SEP model to pure gas permeance as a function of temperature were subsequently used in the model to predict the permeance as a function of pressure. The SEMP model used by Burggraaf neglected coverage of the permeating species on the permeate side of the membrane; however, it predicted permeance through silicalite reasonably well. It was necessary to include effects of permeate pressure in the SEP model here, since we maintained a significant permeate pressure ($\approx$ 17 psia) during the single gas flux measurements and did not use a sweep gas in the permeate.

As shown in Figure 2-8, the model predicted the permeance of light gases with reasonable accuracy. The error for the predicted permeances of CH_4, CO_2, H_2 and n-C_4H_{10} compared to the experimental values were 6.53%, 7.24%, 7.02% and 20.3% respectively. Smaller errors were expected in for gases that adsorb in the Henry regime, because they exhibit little pressure dependence. The error in the fit for n-C_4H_{10}, shown in Figure 2-9, is possibly a result of changes in the ODS layer over time, since a period of approximately 2 months passed between the experiments for pressure and temperature dependence. Also, a more accurate fit of the Langmuir model to the adsorption phenomena of n-C_4H_{10} with respect to the ODS modified membrane could improve the prediction of the trend, including the maximum, for permeance as a function of mean trans-membrane pressure.

The agreement in the fit to this model indicates that the mechanisms of transport in this membrane are similar to those seen in other materials including surface flow, activated configurational diffusion and solution diffusion. The chemical environment of the ODS membrane provided a model surface flow material where surface enhanced permeation was responsible for the reverse selectivity for n-C_4H_{10} and CO_2 over

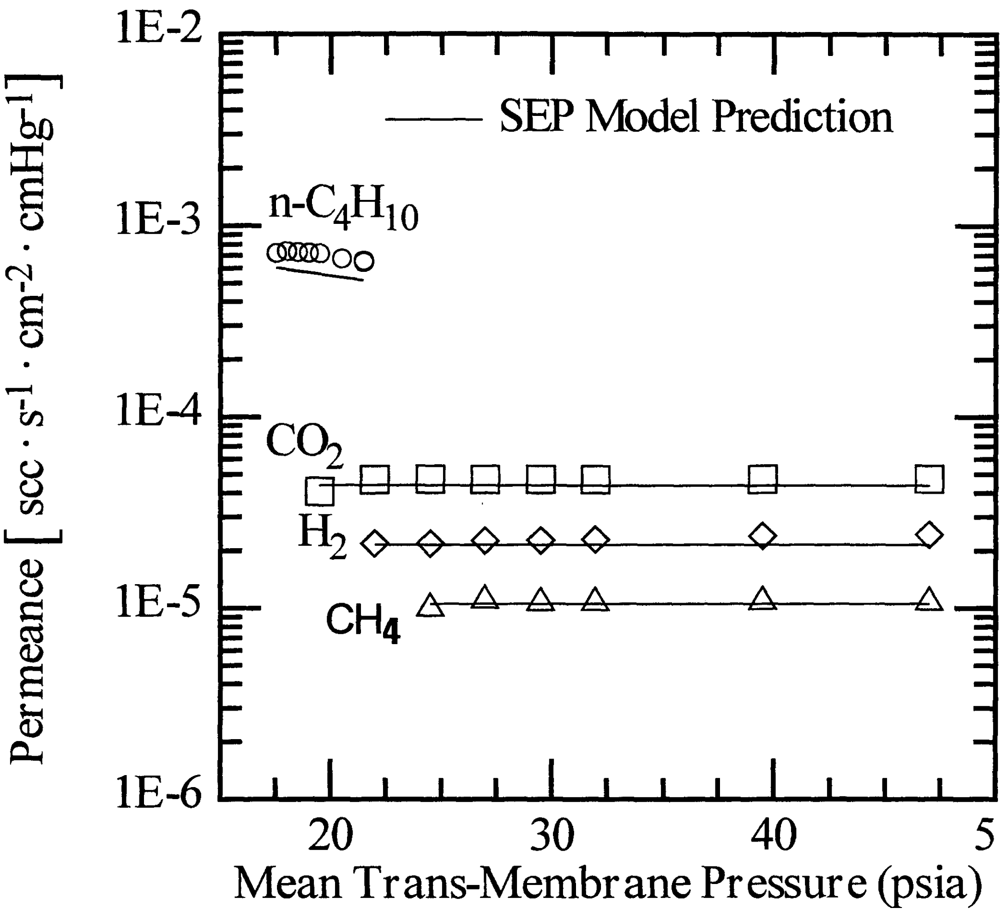

Figure 2-8: Prediction of the pressure dependence of permeance using the SEP model. Light gases exhibit insignificant pressure dependence that is typical for transport in the Henry regime. Transport in the Langmuir regime exhibits significant pressure dependence indicating the presence of vapor phase flow.

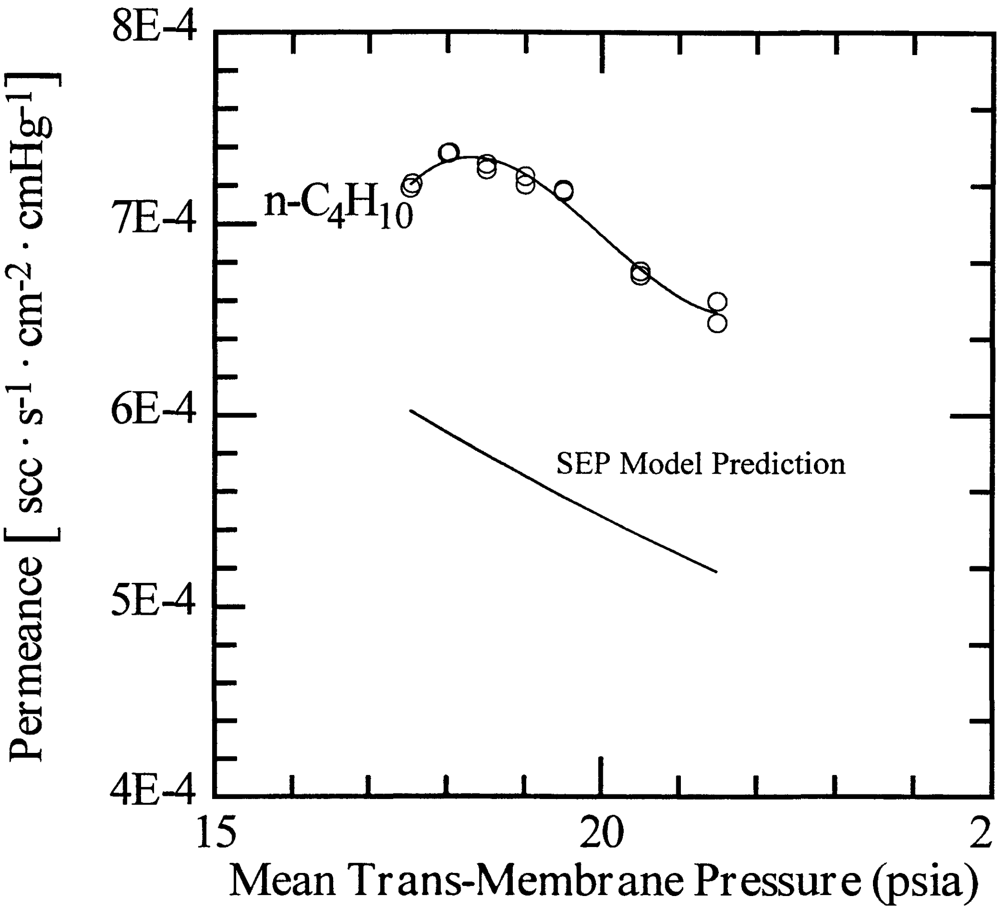

Figure 2-9: SEP model prediction of n-C_4H_{10} permeance as a function of pressure. This is an exploded view of the n-C_4H_{10} data shown in Figure 2-8.

non-condensable gases and light hydrocarbons. In addition, the fit of pure gas permeance with critical temperature, shown in Figure 2-5, is consistent with solution diffusion phenomena. Therefore, the ODS membrane exhibits mechanisms of transport characteristic of both porous and dense membrane materials. Since the morphology of the ODS modified membrane is not well understood, it is impossible to classify this material as porous or dense.

2.5 Conclusions

In this chapter we describe a reverse selective gas separation membrane and model surface flow materials fabricated by depositing ODS onto porous alumina. Transmission FTIR analysis of the Anodisc sample were consistent with the hindered motion of alkyl-silanes coupled with the surface. An ODS layer with uniform coverage and a thickness of $\approx$10.1 nm was measured using ellipsometry. Two species of silicon were identified by XPS analysis; one bonded to the sapphire surface and an overlying bulk silane layer. From these observations we hypothesized that the composite membrane contained a very thin selective polymer film of ODS molecules interconnected with the porous alumina surface. However, the ODS modified membrane could consist of pores filled with cross-linked ODS, or a thin ODS film on the surface of the porous substrate.

The permeance of the ODS membrane was observed to be history dependent, with increases as high as 30% and decreases of 71% noted over a 16-month period. However, membrane in toluene and drying at 60 °C, or by exposure to flowing nitrogen at approximately 5.0 psig.

Pure gas permeances for the ODS membrane were approximately two to three orders of magnitude lower than for the unmodified sample. Pure gas permeances followed an exponential relationship with critical temperature, which was evidence of transport strongly influenced by preferential adsorption. Reverse selectivity was observed for all of the condensable gases including n-C_4H_{10}, i-C_4H_{10}, CO_2 and C_2H_6, with selectivities as high as 24 for n-C_4H_{10}/CH_4 and 48 for n-C_4H_{10}/N_2. An increase in mixed gas selectivities over pure gas selectivities for n-C_4H_{10}/C_2H_6 (increasing from 7.0 to 10.8) and for n-C_4H_{10}/CH_4 (increasing from 19.6 to 24) was evidence that competitive adsorption occurred.

The fit of experimental permeance data to the SEP model was consistent with transport of n-C_4H_{10} in the Langmuir adsorption regime, and transport of H_2, CO_2 and CH_4 in the Henry adsorption regime. The ODS membrane exhibited characteristics of transport through both porous (i.e., surface flow and configurational diffusion) and dense (solution diffusion) membrane materials and with the current data it is impossible to classify this material as porous or dense.

2.6 Nomenclature

A	pre-exponential factor
D_c	intrinsic diffusion coefficient
D_F	Fickian diffusion coefficient
E_d	intrinsic activation energy of diffusion
E^+	apparent activation energy of diffusion
J	flux
L	membrane thickness
M	molecular weight of species
K	Langmuir coefficient
p	pressure
Δp_i	partial pressure driving force for species i
P	permeance
q	gas adsorbed per unit sorbent (by surface area or volume)
q_s	gas adsorbed per unit sorbent at saturation
Q_a	isosteric energy of adsorption
R	gas constant
T	temperature
z	distance coordinate

Greek Symbols

$\alpha_{i/j}$	selectivity for species *i* over species *j*
μ^*	geometric correction factor
θ	occupancy

Indices

f	feed
i	species *i*
j	species *j*
o	pre-exponential coefficient
p	*permeate*
r	residue

2.7 References

1. A. L. Jadhav, K. P. Naikwadi, S. Rokushika, H. Hatano, and M. Ohshima, *Journal of High Resolution Chromatography & Chromatography Communications* **10,** 77-81 (1987).
2. M. Ho, M. Cai, and J. E. Pemberton, *Analytical Chemistry* **69,** 2613-2616 (1997).
3. B. Buszewski, R. M. Gadzala-Kopciuch, M. Markuszewski, and R. Kaliszan, *Analytical Chemistry* **69,** 3277-3284 (1997).
4. K. Kimata, K. Hosoya, N. Tanaka, T. Araki, R. Tsuboi, and J. Haginaka, *Journal of Chromatography* , 19-30 (1991).
5. K. P. Naikwadi, A. M. McGovern, and F. W. Karasek, *Canadian Journal of Chemistry* **65,** 970-975 (1987).
6. L. C. Sander, M. Schneider, S. A. Wise, and C. Woolley, *Journal of Microcolumn Separations* **6,** 115-125 (1994).
7. T. Okubo and H. Inoue, *AICHE Journal* **34,** 1031-1033 (1988).
8. J. R. Miller and W. J. Koros, *Separation Science and Technology* **25,** 1257 - 1280 (1990).
9. R. P. Castro, Y. Cohen, and H. G. Monbouquette, *Journal of Membrane Science* **115,** 179-190 (1996).
10. R. P. Castro, Y. Cohen, and H. G. Monbouquette, *Journal of Membrane Science* **84,** 151 (1993).
11. S. H. Hyun, S. Y. Jo, and B. S. Kang, *Journal of Membrane Science* **120,** 197-206 (1996).
12. M. B. Rao and S. Sircar, *Journal of Membrane Science* **85,** 253-264 (1993).
13. C. Leger, H. D. L. Lira, and R. Paterson, *Journal of Membrane Science* **120,** 135-146 (1996).
14. C. Leger, H. D. L. Lira, and R. Paterson, *Journal of Membrane Science* **120,** 187-195 (1996).
15. P. Mejean, A. Collet, M. Viguier, A. Sivade, D. Bourret, and A. Larbot, in *ICIM 5* (Japan, 1998), pp. 176-179.
16. A. J. Burggraaf, in *Fundamentals of Inorganic Membrane Science and Technology*, edited by A. J. Burggraaf and L. Cot (Elsevier Science B.V., 1996), pp. 331-431.
17. A. J. Burggraaf, *Journal of Membrane Science* **155,** 45-65 (1999).
18. A. W. Adamson, *Physical Chemistry of Surfaces* (Interscience Publishers, Inc., New York, 1960).

19 Y. H. Ma, in *Fundamentals of Inorganic Membrane Science and Technology*, edited by A. J. Burggraaf and L. Cot (1996).

20 J. C. Slattery, *Momentum, Energy and Mass Transfer in Continua*, second edition ed. (Robert E. Krieger Publishing Company, New York, 1981).

21 M. H. Hassan, Ph.D., Oregon State University, 1994.

22 M. H. Hassan, J. D. Way, P. M. Thoen, and A. C. Dillon, *Journal of Membrane Science* **104,** 27-42 (1995).

23 J. Kärger and D. M. Ruthven, *Diffusion in Zeolites and Other Microporous Solids* (John Wiley and Sons, New York, 1992).

24 E. P. Plueddemann, *Silane coupling agents*, 2nd ed. (Plenum Press, New York, 1991).

25 B. Johs, C. Herzinger, and B. Guenther, , 3.212 ed. (J.A. Woollam, Lincoln, NE, 1998).

26 T. Lichtenstein, *Handbook of Thin Film Materials* (University of Rochester, Rochester, NY, 1979).

27 S. R. Wasserman, Y.-T. Tao, and G. M. Whitesides, *Langmuir* **5,** 1074-1087 (1988).

28 K. M. R. Kallury, M. Cheung, V. Ghaemmaghami, U. J. Krull, and M. Thompson, *Colloids and Surfaces* **63,** 1-9 (1992).

29 C. P. Tripp and M. L. Hair, *Langmuir: the ACS journal of surfaces and colloids* **11,** 149-155 (1995).

30 G. Hollinger and F. J. Himpsel, *Physical Review B* **28,** 3651-3653 (1983).

31 J. B. Brzoska, I. B. Azouz, and F. Rondelez, *Langmuir* , 4367-4373 (1994).

32 C. P. Tripp and M. L. Hair, *Langmuir: the ACS journal of surfaces and colloids* **8,** 1120-1126 (1992).

33 S.-T. Hwang and K. Kammermeyer, *Membranes in Separations* (John Wiley and Sons, New York, 1975).

34 M. Mulder, *Basic Principles of Membrane Technology* (Kluwer Academic Publishers, Boston, 1991).

35 J. W. Bakker, F. Kapteijn, J. Poppe, and J. A. Moulijn, *Journal of Membrane Science* **117,** 57-78 (1996).

36 I. SAS Institute, , 3.2 ed. (Cary, NC, 1997).

37 D. W. Breck, *Zeolite Molecular Sieves: Structure, Chemistry and Use* (Wiley, New York, 1974).

38 F. Kapteyn, W. J. W. Bakker, G. Zheng, and J. A. Moulijn, *Microporous Materials* **3,** 227-234 (1994).

39 F. Kapteyn, W. J. W. Bakker, J. v. d. Graaf, G. Zheng, J. Boppe, and J. A. Moulijn, *Catalysis Today* **25,** 213-218 (1995).

40 F. Kapteyn, W. J. W. Bakker, G. Zheng, J. Boppe, and J. A. Moulijn, *Chemical Engineering Journal* **57,** 145-153 (1995).

41 J. P. Collins, J. D. Way, and N. Kraisuwansarn, *Journal of Membrane Science* **77,** 265-282 (1993).

Chapter 3

Fluorosilane Modified Membranes for Gas and Vapor Separations

3.1 Introduction

A U.S. Filter ultrafiltration membrane modified with octadecylsilane (ODS), in Chapter 2, showed enhanced permeances and reverse selectivity, or selectivity for heavier-gases over lighter gases, due to surface diffusion of hydrocarbons and CO_2. A significant effect on selectivity should be observed by changing the chemical environment of the membrane, by choosing a different silane modification agent. The experiment proposed to further demonstrate the effects of silanization was to use a silane functional group similar to ODS that has been changed simply by replacing methyl-hydrogens with fluorine.

Miller and Koros modified γ-alumina ultrafiltration (UF) membranes with a 4 nm pore diameter using tridecafluoro-1,1,2,2,-tetrahydrooctyl-1-trichlorosilane [1]. The pore size of the UF membrane was reduced to separate low molecular weight liquids, such as solvents from lube oils. Pure gas permeation experiments indicated the modified membrane showed a decrease in permeability of up to 2 orders of magnitude, and a small decrease in selectivity of He over Ar and SF_6 compared to the unmodified membrane. However, the reduction in pore size was not sufficient to prevent the flow of lube oil.

In a subsequent paper, Leger et al. used octadecyltrichlorosilane to modify γ-alumina supports with a pore size of 5 nm for gas separations [2]. The trichlorosilanes reacted with hydroxylated surfaces through a direct substitution reaction that attached the octadecylsilane (ODS) molecules to the surface. Pure gas permeabilities were decreased by 3 orders of magnitude, resulting in reverse selectivity of CH_4/He and CO_2/N_2. They reported the order of permeabilities for the untreated membrane to be He > CH_4 > C_3H_8 > N_2 > CO_2 > Ne > Ar in contrast to the order for the ODS treated membrane CH_4 > He > ($C_3H_8 \cong CO_2$) > N_2 > Ne > Ar. Permeabilities were reduced by a factor of 5 after exposure to a 1 atm N_2 feed with vacuum on the permeate side. They assumed this phenomena to be caused by compaction of the octadecylsilane layer and permeabilities were recovered in the absence of vacuum after several hours, by reversal of the pressure difference, or after rinsing in toluene.

Mejean et al. used dodecyl-triethoxysilane, $(C_2H_5O)_3SiC_{12}H_{25}$, and tridecafluoro-1,1,2,2-tetrahydro-octyloxypropyl-triethoxysilane, $(C_2H_5O)_3SiO(CH_2)_3C_6F_{13}$, separately to modify γ-alumina membranes with a pore size of 5 nm [3]. Single gas permeability tests for the membrane functionalized with dodecyl-triethoxysilane agreed with their experiments, except that the membrane was selective for CO_2 and C_3H_8 over He. Selectivities of approximately 2-4 for C_3H_8 and CO_2 over N_2 and He were observed. The membrane modified with the fluorinated functional group showed a sharp decrease in the permeability of hydrocarbons, with increased selectivities for CO_2 over C_3H_8 and N_2 of approximately 2.5-3.5. The orders of permeability were $C_3H_8 > CO_2 > He > N_2$ for the dodecylsilane functional group and $CO_2 > He > C_3H_8 > N_2$ for the fluorinated functional group.

In this chapter, a mesoporous alumina ultrafiltration membrane was modified with heptadecafluoro-1,1,2,2-tetrahydrodecyl-trichlorosilane (HDFS), $Cl_3Si(C_2H_4)C_8F_{17}$. Mixed gas separations and pure gas permeation measurements were performed with HDFS membrane, and a correlation between permeance and the relevant physical properties of gases was used to show the mechanisms of transport through the membrane. This study was meant as a demonstration of a change in the order of selectivity for CO_2 over hydrocarbons by changing the chemical nature of the membrane, in comparison with the octadecyltrichlorosilane (ODS) membrane described in Chapter 2. A surrogate porous alumina sample was also modified for transmission FTIR analysis to confirm the presence of the HDFS layer.

3.2 Experimental

Asymmetric γ-alumina ultrafilters (U.S. Filter T-170, Warrendale, PA) with a mesoporous top layer were modified using HDFS. Silanization and transport experiments were performed following the same procedures used for the study of the ODS membrane in Sections 2.3.1 and 2.3.3. Transmission Fourier transform infrared spectroscopy (FTIR) was performed using a Biorad (Cambridge, MA) FTS 40 FTIR to confirm the presence of HDFS layer deposited on the surface of a surrogate sample (Anodisc alumina ultrafilters, 0.2 μm; Whatman, Inc., Hillsboro, Oregon) following the procedures in Section 2.3.2.1.

Toluene was used as the solvent during the silanization steps for both the HDFS and ODS membranes. In hindsight, it was recognized toluene is not the preferred solvent for fluorosilanes, because of the solubility of HDFS is low [4]. Therefore more appropriate methods for the deposition of HDFS include the use of aprotic fluorinated-hydrocarbons as solvents (i.e., Freon 113 [3]), or the trichlorosilane can be used in the vapor phase as described by Miller et al. [1].

3.3 Results and Discussion

3.3.1 *Transmission FTIR Spectroscopy*

The transmission-FTIR spectra for an Anodisc after modification with HDFS using an unmodified Anodisc for background, is given in Figure 3-1. Referencing the spectra to an unmodified Anodisc isolated the sharp fluorocarbon peak that confirms modification with HDFS. This was necessary to observe the fluorocarbon stretches ($-CF_3$ and $-CF_2-$) between 1000 and 1350 cm^{-1} that are adjacent to the upper limit of adsorption around 1200 cm^{-1} due to Al_2O_3.

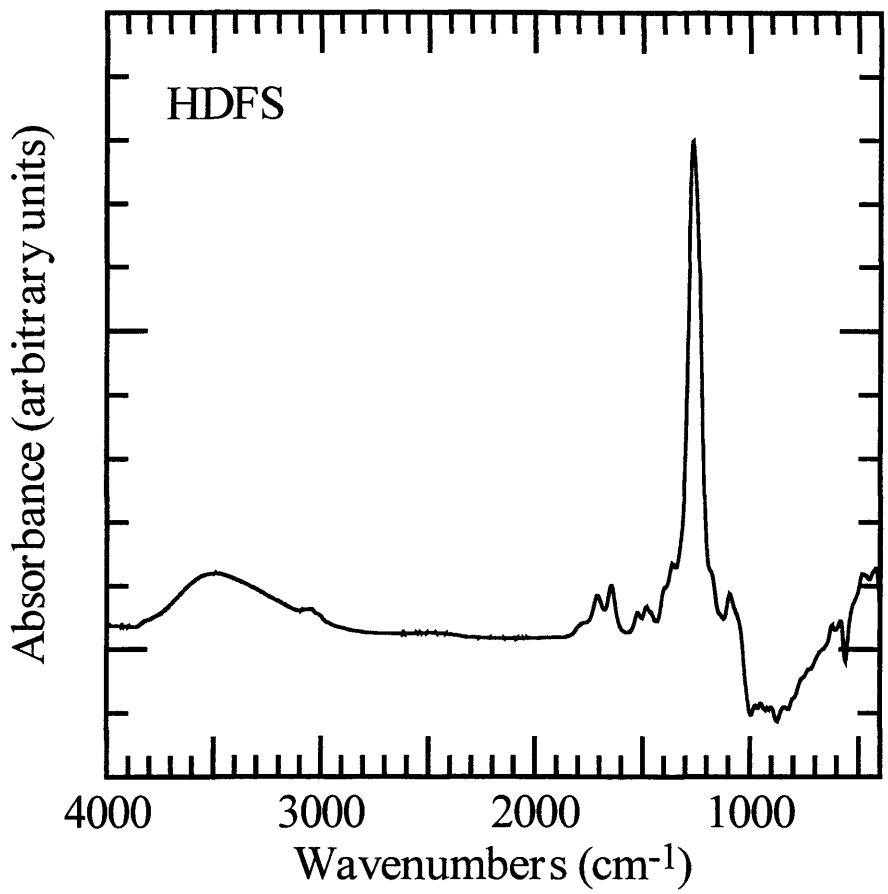

Figure 3-1: Transmission FTIR spectra for a 0.2 μm Anodisc modified with HDFS referenced to the sample before modification. The sharp $-CF_2$ and $-CF_3$ stretches seen between 1000 and 1350 cm^{-1} indicate the hindered motion of fluorinated-alkylsilanes grafted onto the surface.

3.3.2 *Permeance of the HDFS Membrane*

Pure gas permeance and selectivity were used to gauge the integrity of the 5 nm alumina membrane (U.S. Filter, T-170) and to set a baseline for the sample's performance prior to silanization, as discussed in Section 2.4.1. Knudsen diffusion and surface diffusion were the dominant transport mechanisms, and reverse selectivity was observed for the unmodified substrate. This analysis showed that there were no significant defects, and that the U.S. Filter membrane was a good substrate for the investigation of how the chemistry of silanes influences membrane properties.

Table 3-1 summarizes the pure gas and mixed gas permeances and selectivities of the HDFS membrane. The ratios of the permeances are presented for easy comparison with the respective selectivities for each mixture. Pure gas permeance measurements were performed at 293 K with a feed pressure of approximately 32.0 psia and permeate pressure of approximately 17.0 psia. Mixed gas separations were performed at 293 K with a feed pressure of approximately 47.0 psia and permeate pressure of approximately 17.0 psia. Mass flow controllers were used to provide binary feed mixtures containing 20 ±2 % CO_2 and the composition of each mixture was checked with the gas chromatograph. Pure gas experiments were performed during a two-day period and mixed gas experiments were completed during a period of six weeks.

Properties of the HDFS membrane changed irreversibly during permeation experiments that were performed over a range of temperatures, from 273 K to 353 K. The initial CO_2/H_2 selectivity of 1.6 for the HDFS membrane decreased to 0.56 after one temperature cycle. It appeared that the HDFS layer continued to change during subsequent temperature cycles, therefore data showing the change in permeance as a function of temperature were not reproducible and are not presented. Also, the mixed gas permeances of CO_2 versus n-C_4H_{10} are not shown in Table 3-1, because the experiment was not completed prior to the temperature cycles that changed the membrane.

Table 3-1: Summary of pure and mixed gas permeances for gas mixtures studied with the HDFS membrane. All permeances are given in cgs units ($scc \cdot s^{-1} \cdot cm^{-2} \cdot cmHg^{-1}$) × 10^{-4}.

Mixtures	Ratio of Pure Gas Permeances	Pure Gas Selectivity	Ratio of Mixed Gas Permeances	Mixed Gas Selectivity
CO_2/H_2	0.333/0.204	1.6	0.702/0.307	2.3
CO_2/N_2	0.333/0.071	4.7	0.367/0.070	5.2
CO_2/ CH_4	0.333/0.061	5.4	0.875/0.089	9.8
CO_2/n-C_4H_{10}	0.333/0.025	13.3	n/a	n/a

Modification of the U. S. Filter membrane with HDFS resulted in a decrease in permeance of 3 to 4 orders in magnitude. The membrane was selective for CO_2/n-C_4H_{10}, and reverse selectivity was shown for CO_2 over H_2, N_2 and CH_4. The order of permeance of the HDFS membrane (i.e., $CO_2 > H_2 > N_2 > CH_4 > SF_6 >$ n-C_4H_{10}) was consistent with the results reported by Mejean et al. for a similar fluorosilane modified membrane.

It is often observed that the selectivities of mixed gas separations are higher than pure gas selectivities for microporous [5]. This is attributed to competitive adsorption, where gases that adsorb more strongly block adsorption and reduce the diffusion of other gases. Increases in selectivity with mixed gases observed for the HDFS membrane were 10.6% for CO_2/N_2, 43.8% for CO_2/H_2 and 81.5% for CO_2/ CH_4. These increases were consistent with the competitive adsorption of CO_2.

For the HDFS membrane, increased selectivities for mixed gases accompanied an increase in permeance for all of the gases, except N_2, as high as 160% for CO_2 and 50% for CH_4. This behavior was similar to the behavior of the ODS membrane (Section 2.3.4) where increases in selectivity occurred for mixed gases, but no specific trends were observed. These changes in permeance with respect to selectivity were not consistent with those observed in literature. Rao and Sircar [5] reported that the reverse selectivity of nanoporous carbon membranes for n-C_4H_{10} originated from competitive adsorption that was correlated with a decrease in permeance of the least interacting gases, while the permeance of n-C_4H_{10} was relatively constant. The difference in behavior of the silane modified membranes compared to carbon membranes is a result of differences in membrane material properties. The carbon membrane provides a rigid pore structure, while polymers are known to swell and increase in internal free volume with adsorption [6-8]. An increase in free volume for a polymer is analogous to an increase in pore diameter for porous materials.

The mechanisms of transport through a membrane can be examined by plotting permeance against relevant physical properties of various gases [7,8]. Semilog plots of the pure gas permeances through the HDFS and ODS membranes versus kinetic diameter of various gases are given in Figure 3-2. The kinetic diameter is an estimate of the effective cross-sectional area of a molecule and is proportional to the activation energy for configurational diffusion [9]. Therefore, the exponential decrease in permeance of the HDFS membrane with kinetic diameter, as observed in Figure 3-2A, resulted from transport limited by size or shape. A solid line was fit to the lighter gases and hydrocarbons to illustrate the trend. CO_2 and SF_6 were not included in the trend because transport of these gases appeared to be enhanced by surface flow, which was expected due to interactions between the gases with polarizable alkyl-fluoride functional groups.

In contrast, permeance with kinetic diameter through the ODS membrane increased with kinetic diameter, as shown in Figure 3-2B. An increase in permeance with kinetic diameter reveals that the heavier gases permeate fastest. By intuition this could be an indication of surface flow; however the surface flow phenomenon was illustrated better by plotting permeance versus critical temperature, as shown in Figure 2-4.

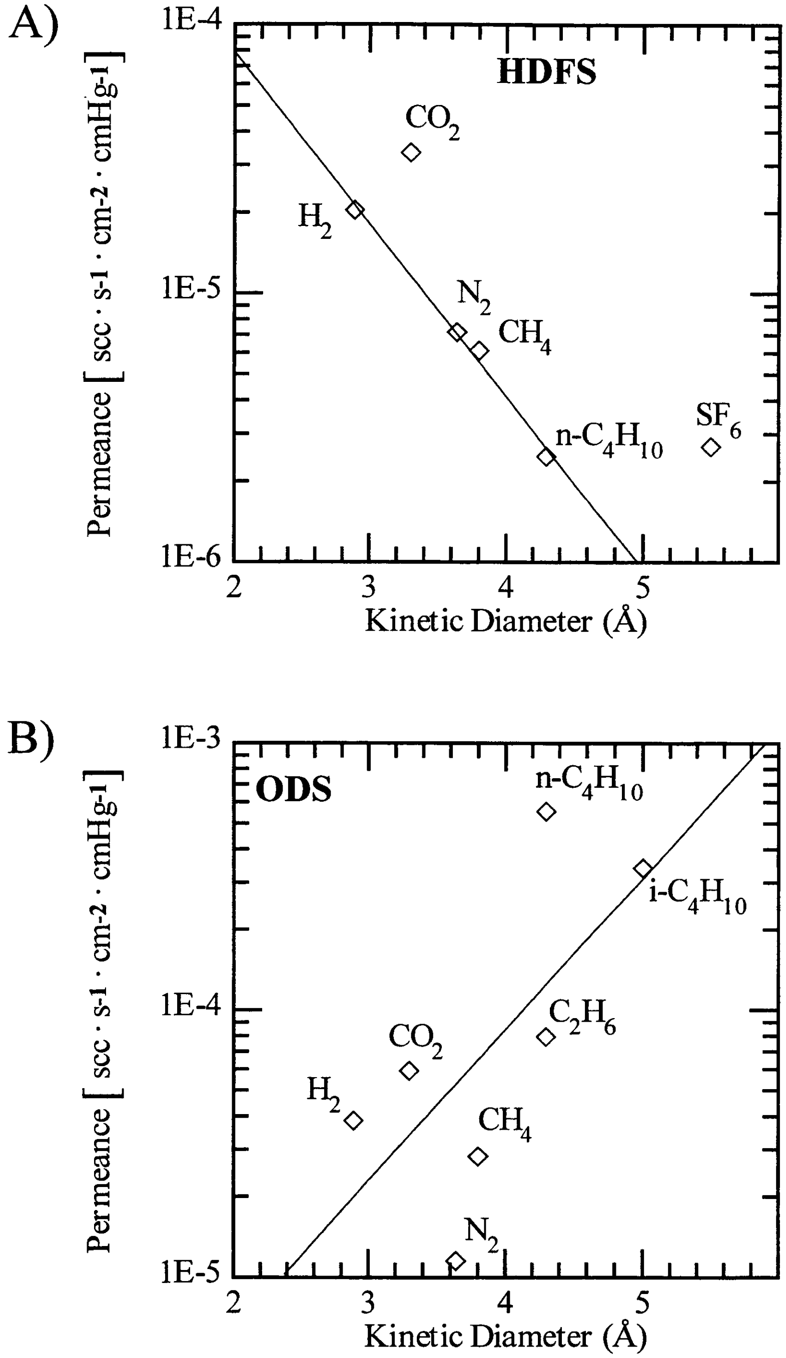

Figure 3-2: Single gas permeances of (A) HDFS and (B) ODS membranes as an exponential function of kinetic diameter.

Although the microstructure of the ODS and HDFS layers are not known, the functional groups consist of monomers that make up common polymers, as shown in Figure 3-3. The structure of the ODS membrane is similar to that of polyethylene, which is known to be a flexible, or rubbery, polymer with a glass transition temperature of approximately 153 K [10]. The HDFS membrane is similar to molecular polytetrafluoroethylene, which is a stiffer, glassy polymer with a glass transition temperature of approximately 399 K [10]. Transport through membranes composed of rubbery polymers are known to be dependent on preferential sorption, while transport through membranes composed of glassy polymers are known be dependent on the size and shape of the diffusing molecule [6,8].

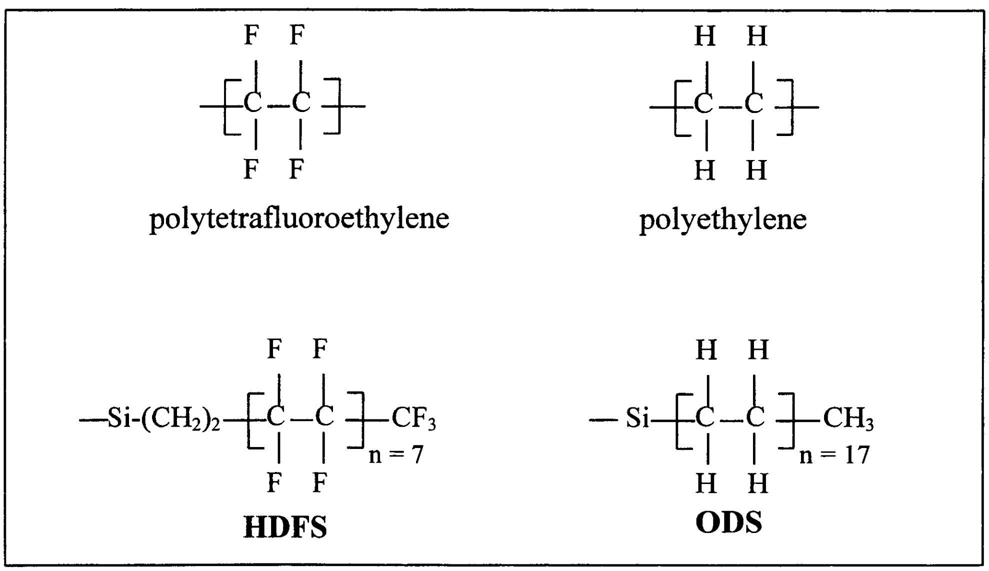

Figure 3-3: The chemical structures of the functional groups HDFS and ODS are composed mainly of the same monomers as polytetrafluoroethylene and polyethylene.

3.3.3 *Changing Chemistry of Silane Modification Changes the Order of Selectivity*

A summary of the pure and mixed gas CO_2 selectivities of the HDFS and ODS membranes (Sections 2.4.3 and 2.4.4) are given in Table 3-2. For comparison, the pure gas permeances of CO_2 were 3.33 x 10^{-5} (scc·s $^{-1}$·cm^{-2} ·cmHg) and 5.91x 10^{-5} (ssc·s $^{-1}$·cm^{-2} ·cmHg) for the HDFS and ODS membranes, respectively. The reverse selectivities observed for CO_2 over H_2 and N_2 were similar for both the ODS and HDFS membranes.

Table 3-2: A summary of selectivities for the ODS and HDFS membranes.

Mixture	**ODS Membrane Selectivity**		**HDFS Membrane Selectivity**	
	Pure Gas	**Mixed Gas**	**Pure Gas**	**Mixed Gas**
CO_2/H_2	1.5	1.4	1.6	2.3
CO_2/N_2	5.1	5.7	4.7	5.2
CO_2/CH_4	2.1	4.4	5.4	9.8
$CO_2/n\text{-}C_4H_{10}$	0.107	0.093	13.5	NA

The most significant difference in performance between the ODS and HDFS membranes was the change in the order of selectivity for CO_2 to hydrocarbons. The $CO_2/n\text{-}C_4H_{10}$ selectivity was 13.5 for the HDFS membrane and 0.107 for the ODS membrane, therefore the pure gas selectivity for $CO_2/n\text{-}C_4H_{10}$ was over 100 times greater with the HDFS membrane. The HDFS membrane had a higher affinity for CO_2 and separates gases based on size, while the ODS membrane had a high affinity for hydrocarbons that resulted in very high permeances of butane. This change in the order of selectivity for CO_2 with relation to hydrocarbons was a convincing demonstration of the effect of surface modification on membrane performance.

3.4 Conclusions

A CO_2 selective membrane was fabricated by silanization of a mesoporous alumina membrane with HDFS. Transmission FTIR spectra were consistent with the presence of HDFS deposited on surrogate porous alumina samples. Properties of the HDFS membrane changed irreversibly during experiments performed over a range of temperatures, from 273 K to 353 K. The initial CO_2/H_2 selectivity of 1.6 for the HDFS membrane decreased to 0.56 after one temperature cycle.

The HDFS membrane showed reverse selectivity for CO_2 over H_2, N_2, CH_4 and n-C_4H_{10} due to configurational effects and surface diffusion. An exponential decrease in the permeance of the HDFS membrane with kinetic diameter resulted from transport limited primarily by configurational effects. Also, increases in selectivity for mixed gases relative to pure gases was evidence that transport of CO_2 enhanced by surface diffusion.

A change in the order of selectivity for CO_2 over hydrocarbons was achieved by modifying mesoporous alumina membranes with HDFS as opposed to ODS. The

CO_2/n-C_4H_{10} selectivity was 13.5 for the HDFS membrane and 0.107 for the ODS membrane, therefore the pure gas selectivity for CO_2/n-C_4H_{10} was over 100 times greater with the HDFS membrane. The HDFS membrane has a higher affinity for CO_2 and separates gases based on size, while the ODS membrane has a high affinity for hydrocarbons that results in very high permeances of n-C_4H_{10} by surface diffusion. The change in the order of selectivity for CO_2 with relation to hydrocarbons is a convincing demonstration of the effect of surface modification on membrane performance.

3.5 References

1 J. R. Miller and W. J. Koros, *Separation Science and Technology* **25,** 1257 - 1280 (1990).

2 C. Leger, H. D. L. Lira, and R. Paterson, *Journal of Membrane Science* **120,** 187-195 (1996).

3 P. Mejean, A. Collet, M. Viguier, A. Sivade, D. Bourret, and A. Larbot, in *ICIM 5* (Japan, 1998), pp. 176-179.

4 *CRC Handbook of Chemistry and Physiscs*, Vol. , edited by R. C. Weast, M. J. Astle, and W. H. Beyer (CRC Press, Inc., Boca Raton, 1986).

5 M. B. Rao and S. Sircar, *Journal of Membrane Science* **85,** 253-264 (1993).

6 W. S. W. Ho and K. K. Sirkar, *Membrane Handbook* (Van Nostrand Reinhold, New York, 1992).

7 S.-T. Hwang and K. Kammermeyer, *Membranes in Separations* (John Wiley and Sons, New York, 1975).

8 M. Mulder, *Basic Principles of Membrane Technology* (Kluwer Academic Publishers, Boston, 1991).

9 D. W. Breck, *Zeolite Molecular Sieves: Structure, Chemistry and Use* (Wiley, New York, 1974).

10 Z. Tadmor and C. G. Gogos, *Principles of Polymer Processing* (John Wiley and Sons, New York, 1979).

Chapter 4

Separation of Xylene Isomers by Pervaporation

4.1 Introduction to Xylene Separations

At a production value of approximately $4 billion in 1996, mixed xylenes are ranked second in world consumption of aromatic products behind benzene and toluene [1]. Most of the mixed xylenes are separated into the three isomers o-, m- and p-xylene that are oxidized to their corresponding dibasic aromatic acid or anhydride (phthalic anhydride, isophthalic acid and terephthalic acid). A significant portion of p-xylene is converted to the dimethyl ester of terephthalic acid. The major end uses of these intermediates are polymeric materials including polyvinyl chloride (PVC), polyester resins and polyethylene terephthalate (PET). p-Xylene is the isomer with the largest demand that is growing at 7% annually [1].

Successful chemical separations take advantage of differences of the physical properties of compounds. The cost of separations increases when the components of a mixture have similar properties. Isomeric separations (i.e., o-, m- and p-xylene) are especially challenging because of similarities in bulk properties, such as vapor pressure and solubility; therefore it is necessary to focus on differences in physical properties, such as melting points, dipole moments and molecular geometry.

Table 4-1 summarizes vapor pressures and properties that distinguish the three isomers of xylene. The boiling point of o-xylene is about 5 K higher than for the other isomers, therefore it can be separated from the mixed xylenes directly by fractional distillation. The difference in vapor pressures between m-xylene and p-xylene is less than 1 K, making vapor liquid equilibrium (VLE) separations (i.e., distillation) of these two isomers expensive. The relative volatilities, defined as the ratio of the vapor pressures, for p-xylene to o-xylene and m-xylene are 1.34 and 1.06, respectively[i]. It is necessary to achieve a separation factor greater than the relative volatility to compete with VLE processes. The separation factor defined in mole fractions in the feed (x) and product streams (y) of components i and j is given below:

$$\alpha_{i/j} = \frac{y_i / y_j}{x_i / x_j} \tag{4.1}$$

The product stream described for this separation factor is permeate from a membrane process or the adsorbed phase from an adsorption process [2].

The most common method for xylene separation has been by first the separating o-xylene by distillation, followed by crystallization to separate m-xylene and p-xylene. However, the presence of a eutectic point for the binary mixture limits recovery of p-xylene to 60 – 65% per pass before a solid solution forms, which increases the energy

---

[i] *It is reasonable to define the relative volatility as the ratio of the vapor pressures in this case, because the experiments were performed over a narrow range of concentration consisting of approximately 1/3 parts of each isomer at low pressure.*

required and the total fixed capital cost [3,4]. Since the p-xylene produced by the crystallization process is essentially pure, efforts to improve the crystallization process are being pursued.

Table 4-1: Properties of xylene isomers.

	o-xylene	**m-xylene**	**p-xylene**
Geometry	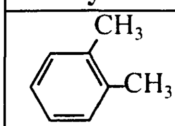	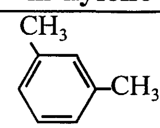	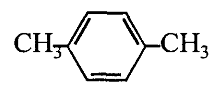
Kinetic Diameter [5] (nm)	0.680	0.680	0.585
Boiling Point[4] @ 101.3 kPa (K)	417.56	412.27	411.52
Vapor Pressure [6] @ 293 K (kPa)	0.659	0.832	0.883
Melting Point [7] (K)	248.0	225.2	286.4
Dipole Moment[8] (Debye)	0.62	0.37	0

Adsorption processes are promising because they allow recovery of 95% or higher per pass [4]. In these processes separation is accomplished by taking advantage of the differences in affinity of p-xylene for the adsorbent relative to other isomers. Sorbents are selective by steric effects, molecular sieving, and/or solubility, while separation processes can be operated in an equilibrium limited mode or a diffusion (kinetic) limited mode [9]. To operate efficiently, the newer adsorption technologies required the design of a complex simulated countercurrent moving bed process. As of 1996 there were only three commercialized p-xylene adsorption processes: UOP's Parex, IFP's Eluxyl and Toray's Aromax[4].

Pervaporation, a membrane process that separates vapor from a liquid feed, has been employed successfully for organic/aqueous separations and is of interest for xylene separations [2,10]. The materials used for pervaporation membranes are similar to sorbents in that they are selective based on steric effects and chemical affinity rather than volatility. In theory, the energy consumption and total fixed capital are much less for pervaporation compared to competing processes [2]. The obstacle to commercializing pervaporation for xylene separations, as with other organic/organic separations, is the identification and development of a suitable membrane.

Dense polymers [8,11-14] and zeolites [15-17] are being investigated as membrane materials for xylene separations. Except for a few noted exceptions, the results can be summarized in three statements; first, a promising selectivity indicated by permeation rates of pure components may not be achieved during separations from a mixture. Secondly, the selectivity observed during a pervaporation experiment is highly dependent on conditions, such as temperature and feed concentration. Finally, many of the selectivities that are reported in literature are very comparable to the relative volatility of the xylene isomers. Matsukata and Kikuchi observed a selectivity of approximately 2.5 for p-xylene/o-xylene from a binary mixture at 303 K using a FER zeolite membrane [16].

This selectivity is significant when compared to a relative volatility of 1.34 for the mixture.

To correct for the separation that occurs by evaporation during pervaporation, the selectivity of the membrane can be estimated by dividing the selectivity from equation (4.1) by the relative volatility, as given below:

$$\alpha^*_{i/j} = \left(\frac{y_i / y_j}{x_i / x_j} \right) \times \frac{1}{p_i^* / p_j^*} \tag{4.2}$$

In this case, the relative volatility is taken as the ratio of the vapor pressures (p^*), and the superscripts *F* and *P* refer to the feed and permeate streams, respectively [2,13,18]. By equation (4.2) the p-xylene/o-xylene selectivity observed for the FER membrane is 1.8. This approach is physically relevant, although it is not thermodynamically consistent over a broad range of temperatures, pressures and concentrations.

Wytcherley and McCandless observed selectivities ranging from 0.833 to 20 for p-xylene/m-xylene by pervaporation with a polypropylene membrane depending on temperature, concentration and the addition of CBr_4 as a complexing agent [14]. Most significantly, experiments performed with 90% p-xylene feed at 253 K, with or without the addition of CBr_4, showed a m-xylene/p-xylene selectivity of 20. The membrane became selective for p-xylene between 268 and 278 K, but leveled out at p-xylene/m-xylene selectivities of 1.1 to 1.2. By complexing p-xylene with CBr_4 they were able to maintain selectivity for m-xylene to higher temperatures up to 313 K.

The focus of this work was to initiate a study of the separation of xylenes by pervaporation and screen potential membranes. We performed pervaporation experiments using a ternary feed mixture with equal parts o-xylene, m-xylene and p-xylene under ambient conditions. We chose four tubular membranes that were available in the lab, including two zeolite membranes and two silane-modified membranes.

4.2 Experimental

4.2.1 *Materials*

Four membranes made of four different materials were screened for their ability to separate xylenes by pervaporation under ambient conditions. The two of zeolite membranes were obtained through research in cooperation with TDA Research (TDA Research, Wheatridge, CO), including MFI silicalite and ZSM-5. These membranes were comprised of thin zeolite layers deposited onto the surface inside of the bore of a macroporous (approximately 0.2 μm) alumina tube. The ODS and HDFS were fabricated as described in Chapters 2 and 3.

4.2.2 *Measurement of Pure Gas Selectivity*

Pure gas fluxes were measured for the membranes prior to pervaporation experiments using a steady-state permeance method [19]. Feed and permeate pressures were set using backpressure regulators and permeate flow rates were measured using bubble flow meters. Cross flow feed was maintained through the bore of the tubular sample using mass flow controllers at moderate flow rates (10 – 20 sccm).

The samples were mounted with Viton o-rings into a stainless steel shell and tube flow cell (see Figure 2-2). The Ar, H_2 and N_2 used for transport experiments was 99.999% pure (General Air, Denver, CO), while SF_6 was at least 99.0% (Scott Specialty Gases, Longmont, CO). The gases were used without further purification.

4.2.3 *Pervaporation*

Pervaporation was performed at room temperature in the apparatus described in Figure 4-1. Cross flow of the liquid feed was provided at a range of 100 to 125 ml/minute using a laboratory pump. Vacuum was maintained below 1 Torr on the permeate side using a vacuum controller, which is the lower limit of the controller. Two cold traps were used in parallel between the sample and vacuum pump to collect permeate. Valves were used to switch between cold traps so that a one hour start-up period was allowed before collecting a permeate sample for analysis. A third back-up cold trap was used to collect permeate that bypassed the main cold traps. No permeate was observed in the back-up cold trap during any of the experiments. A mixture of dry ice and ethanol was used to maintain the cold traps at about 201 K. The permeate was visible as frozen crystals inside the cold trap at this temperature.

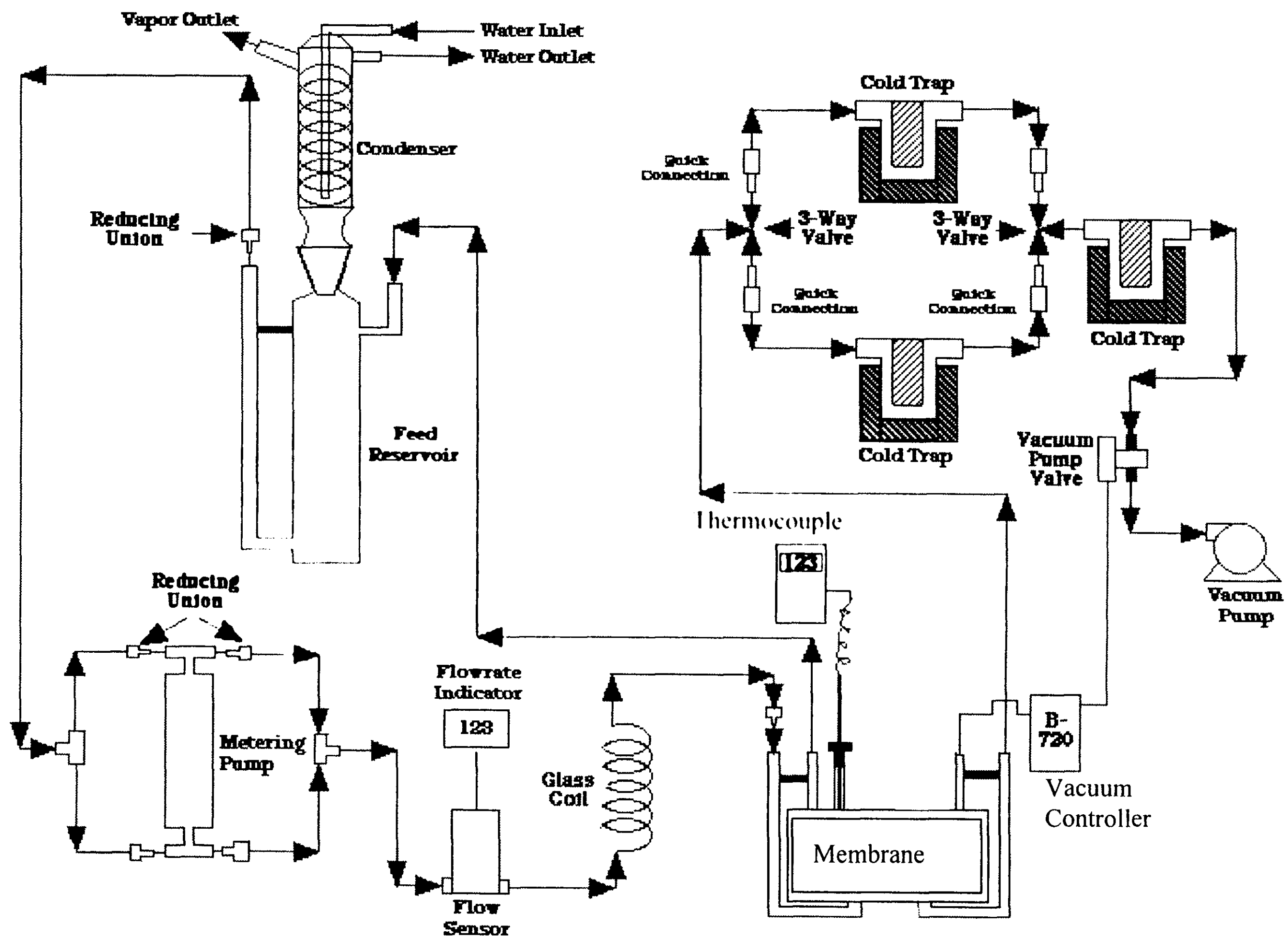

Figure 4-1: Schematic of pervaporation apparatus.

Feed for the pervaporation experiments consisted of approximately equal parts of o-xylene, m-xylene and p-xylene. The anhydrous grade m-xylene was at least 99% pure, HPLC grade p-xylene was at least 99% pure and HPLC grade o-xylene was at least 98% pure (Aldrich , Milwaukee, WI). A total feed volume of 450 to 600 ml was used for each experiment.

The composition of feed, residue and permeate samples for the xylene experiments were determined using a Hewlett Packard 5890 GC with a Hewlett Packard 5970 mass spectrometer (GC-MS). A 30 m long Alltech EC-WAX silica capillary column with an inner diameter of 0.25 mm was used with helium sweep gas. A temperature ramp between 30 °C and 190 °C was used to obtain baseline to baseline separation of all components (see Appendix 3).

Analysis of a standard mixture showed that the signals (peak areas) from the mass spectrometer were approximately equal for all three xylene isomers. Also, we did not observe broad variations in composition, therefore no calibration of the GC-MS was performed. Compositions and selectivities were calculated using a mass balance determined from the peak areas.

4.3 Results

Table 4-2 includes a summary of the separation factors, as defined by equation (4.2), and total fluxes measured for each membrane under ambient conditions (approximately 22 C and 82.6 kPa) with an approximately equimolar o-xylene, m-xylene, p-xylene feed composition. Data are listed in chronological order from top to bottom for the ODS and ZSM-5 membranes. Pure gas selectivities, defined as the ratio of the pure gas permeances, are listed as a baseline comparison for each type of membrane.

Table 4-2: Separation factors and total flux of membranes for separation of xylene isomers by pervaporation. Data are listed in chronological order from top to bottom for the ODS and ZSM-5 membranes.

Membrane	Pure Gas Selectivity	**Separation Factor**: Equation (4.2)			
		O/P	**O/M**	**M/P**	**Total Flux** ($g/s/cm^2$)
ODS	$H_2/N_2 = 3.4$	1.1 1.2	0.9 1.1	1.2 1.0	2.88×10^{-6} 1.19×10^{-5}
HDFS	$H_2/N_2 = 2.9$	1.5	1.4	1.1	1.36×10^{-6}
Silicalite	$Ar/SF_6 = 28$	1.4	1.4	1.0	1.62×10^{-5}
H^+ ZSM-5	$Ar/SF_6 = 2.4$	2.6 2.2 1.4	2.1 2.0 1.3	1.2 1.1 1.0	2.56×10^{-6} 1.99×10^{-6} 3.93×10^{-5}

The H_2/N_2 selectivities for the ODS and HDFS membranes were lower than but comparable to the theoretical Knudsen selectivity of 3.74. It was shown, in Chapters 2 and 3, that gas transport through the ODS membrane was strongly influenced by preferential adsorption, while gas transport through the HDFS membrane was controlled by configurational diffusion. Though the total flux of xylenes was similar for both of the silane-modified membranes, the ODS membrane was essentially non-selective for any of the xylene isomers, while the HDFS membrane exhibited a modest selectivity for o-xylene. The selectivity of the HDFS membrane was not consistent with configurational diffusion, because it was least selective for p-xylene, which has the smallest kinetic diameter. Therefore, it is hypothesized that the selectivity of the HDFS membrane is due to interactions of the more polar o-xylene molecule with the polarizable $-CF_2-$ and $-CF_3$ functional groups. If this hypothesis is true, then grafting of functional groups that are known complexing agents for specific isomers should have a significant affect on selectivity.

The Ar/SF_6 selectivity of the silicalite membrane was over 10 times higher than for the ZSM-5 membrane. The pure gas selectivity did not indicate a trend for the membrane's selectivity for xylenes. The o-xylene selectivity of the silicalite membrane was comparable to the selectivity of the HDFS membrane, however the selectivity of the ZSM-5 membrane was substantially higher. As with the silane-modified membranes, o-xylene appears to have an affinity for the zeolite because it provides the most polar environment. The ZSM-5 membrane is in the hydrogen form, which is characterized by the presence of the H^+ cation within the zeolite structure [20]. If the presence of the proton is responsible for the selectivity of o-xylene, then it is reasonable that ion exchange, say with Na^+, should have a profound affect on selectivity and transport.

Three pervaporation experiments were performed with the ZSM-5 membrane in the hydrogen form to reproduce its selectivity for o-xylene. The o-xylene/p-xylene decreased by 15% after the second experiment. The 15% decrease in selectivity was observed along with a 22 % decrease in flux, indicating a change in the property of the material that was responsible for the selective transport of o-xylene.

A 46% decrease in o-xylene/p-xylene selectivity was observed for the third pervaporation experiment that corresponded with an over an order of magnitude increase in flux. The significant increase in flux and decrease in selectivity were evidence of damage to the ZSM-5 membrane. A difference in sample preparation occurred between the second and third experiments that may be responsible for the damage. Prior to the second experiment, the sample cell was removed from the pervaporation apparatus and placed in a vacuum oven at approximately 250 Torr and room temperature; in contrast the sample was removed from the sample cell and dried in air at 70 ° C prior to the third experiment. Drying before the third experiment was done without a temperature ramp, therefore excessive pressures may have evolved within the microstructure as xylenes vaporized, causing cracks in the zeolite layer.

The membranes of each material type (silane-modified and zeolite) that provided the most polarizable, or most polar environment were responsible for the higher selectivities observed for o-xylene. Configurational effects are a significant influence on diffusion through both materials, however the crystalline structure of the zeolite material may be responsible for the higher selectivity of the ZSM-5 membrane.

4.4 Conclusions

Though the selectivities observed of the HDFS and ZSM-5 membranes for o-xylene are not high, they are respectable for the separation of a mixture with a relative volatility that is close to one. The selectivities for o-xylene/p-xylene were as high as 2.4 for the ZSM-5 membrane. Since the selectivity of xylenes in these materials appears to be induced by interactions of the polar o-xylene molecule with polar or polarizable surfaces, it may be possible to improve the membrane performance. Silane modification can be performed with numerous functional group that may interact more strongly with specific xylene isomers. Also, ion exchange should have a significant influence on the selectivity of ZSM-5 for o-xylene.

The loss of selectivity in the ZSM-5 membrane for o-xylene was a result of improper sample preparation. Drying the membrane at 70 °C without a temperature ramp may have caused excessive pressures as xylenes vaporized within the microstructure, causing cracks in the zeolite layer. Drying the sample in a vacuum oven at approximately 250 Torr and room temperature may have caused a small decrease in selectivity. A better method for drying zeolite membranes would be to place in a covered beaker over activated alumina at ambient conditions.

Observations from literature indicate that the feed concentration and temperature at which pervaporation is performed has a significant affect on a membrane's selectivity for xylenes. It is recommended that future screening experiments cover a range in temperature from about 273 to 313 K [21]. Then, once a promising membrane has been identified study its selectivity over a range of feed compositions.

4.5 Nomenclature

p_i partial pressure of species i

x_i mole fraction of species i in the feed

y_i mole fraction of species i in the permeate

Greek Symbols

$\alpha_{i/j}$ separation factor for species i over species j

Indices

* saturation vapor pressure, or separation factor corrected with relative volatility

4.6 References

1 R. E. Davenport, in *Chemical Economics Handbook* (Stanford Research Institute, Menlo Park, 1997), pp. 456.0000.

2 W. S. W. Ho and K. K. Sirkar, *Membrane Handbook* (Van Nostrand Reinhold, New York, 1992).

3 C. J. King, *Separation Processes*, 2nd ed. (McGraw-Hill Book Company, New York, 1980).

4 D. M. Ruthven, *Encyclopedia of Separation Technology* (John Wiley and Sons, New York, 1997).

5 J. Kärger and D. M. Ruthven, *Diffusion in Zeolites and Other Microporous Solids* (John Wiley and Sons, New York, 1992).

6 T. Boublik, V. Fried, and E. Hala, *The Vapour Pressures of Pure Substances* (Elsevier Scientific Publishing Company, New York, 1973).

7 *CRC Handbook of Chemistry and Physics*, Vol. , edited by R. C. Weast, M. J. Astle, and W. H. Beyer (CRC Press, Inc., Boca Raton, 1986).

8 *Lange's Handbook of Chemistry*, Vol. , edited by J. A. Dean (McGraw-Hill Book Company, New York, 1979).

9 R. T. Yang, *Gas Separation by Adsorption Processes* (Imperial College Press, London, 1997).

10 X. Feng and R. Y. M. Huang, *Ind. Eng. Chem. Res.* , 1048-1066 (1997).

11 A. S. Michaels, R. F. Baddour, H. J. Bixler, and C. Y. Choo, *I & EC Process Design and Development* **1,** 14-25 (1962).

12 M. H. V. Mulder, F. Kruitz, and C. A. Smolders, *Journal of Membrane Science* **11,** 349-363 (1982).

13 J. G. Sikona and F. P. McCandless, *Journal of Membrane Science* **4,** 229-241 (1978).

14 R. W. Wytcherley and F. P. McCandless, *Journal of Membrane Science* **67,** 67-74 (1992).

15 C. D. Baertsch, H. H. Funke, J. L. Falconer, and R. D. Noble, *Journal Physical Chemistry* , 7676-7679 (1996).

16 M. Matsukata and E. Kikuchi, *Bulletin Chemical Society Japan* , 2341-2356 (1997).

17 D. B. Shah and H. Y. Liou, *Surface Science and Catalysis* **84** (1994).

18 S.-T. Hwang and K. Kammermeyer, *Membranes in Separations* (John Wiley and Sons, New York, 1975).

19 M. H. Hassan, J. D. Way, P. M. Thoen, and A. C. Dillon, *Journal of Membrane Science* **104,** 27-42 (1995).

20 D. W. Breck, *Zeolite Molecular Sieves: Structure, Chemistry and Use* (Wiley, New York, 1974).

21 F. P. McCandless, *Ind. Eng. Chem. Prod. Res. Dev.* , 483-488 (1982).

Chapter 5

Conclusions and Recommendations

5.1 Conclusions

This work began by modifying commercially available alumina ultrafiltration membranes with octadecyltrichlorosilane (ODS) and testing the ODS membrane for its performance in gas separations. The next step was to demonstrate that changing the agent for surface modification would change surface diffusion properties and the order of gas selectivity. A fluorinated-alkylsilane was chosen to modify the second membrane, so that the change in chemistry was simply to replace hydrocarbon groups with more polarizable fluorocarbon groups. Finally, pervaporation experiments were performed to assess the effects of the different silane layers on the separation of xylene isomers. Zeolite membranes (silicalite and ZSM-5) were also evaluated for xylene separations during the pervaporation experiments.

The following conclusions were drawn from this work:

5.1.1 *A Model Surface Flow Membrane by Modification of Porous γ-Alumina with Octadecyltrichlorosilane*

1) A tubular γ–alumina membrane with a starting pore diameter of 5 nm (U.S. Filter T-170) was modified with ODS. Permeance of the membrane decreased by approximately two to three orders of magnitude as a result of treatment with ODS.

2) Transmission FTIR analysis of an Anodisc sample showed sharp methyl stretches at wavenumbers between 2850 and 3200 cm^{-1}, which was evidence of the hindered motion of the alkylsilanes coupled with the surface of an Anodisc alumina ultrafilter.

3) Ellipsometry analysis of an ODS layer deposited on a polycrystalline sapphire sample indicated deposition of a layer with a thickness of $\approx$11 nm.

4) XPS analysis of ODS deposited on a flat polycrystalline sapphire disk identified two species of silicon. The change in binding energy relative to oxidation state of silicon was consistent with the deposition of a bulk layer of ODS on a metal oxide surface. No chlorines were present and only one species of carbon was identified.

5) Reverse selectivity was observed for condensable gases (n-C_4H_{10}, i-C_4H_{10}, CO_2 and C_2H_6) over non-condensable gases (H_2, N_2 and CH_4). Reverse selectivities were as high as 48 for n-C_4H_{10}/N_2 and 24 for n-C_4H_{10}/CH_4.

6) Pure gas permeance followed an exponential relationship with critical temperature, which is characteristic of solution diffusion that is strongly influenced by preferential sorption.

7) The permeance of the ODS modified membrane was observed to be history dependent, with increases as high as 30% and decreases of 71% noted over a 16-month period. However, the variations in permeance were reversed to within ±10% of the original value by rinsing in toluene and drying at 333 K, or by exposure to flowing nitrogen with low pressure differentials of about 5.0 psi.

8) The permeance of n-C_4H_{10} exhibits a maximum when plotted against either pressure or temperature. This phenomena was consistent with observations of the surface diffusion of condensable hydrocarbons through microporous materials, such as zeolites [1-3].

9) Permeance of gases that were non-condensable (CH_4 and H_2) or close to critical temperature (CO_2) showed negligible pressure dependence and increased exponentially with temperature.

10) Apparent activation energies (E^+) of diffusion were determined from the fit of the SEP models to permeance as a function of temperature. Values of E^+ were 2.95 for n-C_4H_{10}, -4.95 for CH_4, -3.55 for CO_2 and -3.66 for H_2. The transport of n-C_4H_{10} was consistent with surface diffusion in the Langmuir adsorption regime, while the H_2, CH_4 and CO_2 fit the model with surface diffusion in the Henry regime.

The ODS model exhibited characteristics of transport through both porous (i.e., surface flow) and dense (i.e., solution diffusion) membrane materials. With the surface analysis described in conclusions 2, 3 and 4 it is hypothesized that the membrane consists of a very thin film of ODS grafted to the porous alumina substrate. However, the microstructure of the ODS layer is not well understood.

5.1.2 *Gas Separations with a Membrane Prepared by Modification of Mesoporous γ-Alumina using a Fluorinated-Alkylsilane*

11) A tubular γ–alumina membrane with a starting pore diameter of 5 nm (U.S. Filter T-170) was modified with heptadecafluoro-1,1,2,2-tetrahydrodecyl-trichlorosilane (HDFS). Permeance of the membrane decreased by three to four orders of magnitude as a result of treatment with HFDS.

12) Analysis of the transmission-FTIR spectra showed a sharp fluorocarbon stretch (-CF_3 and -CF_2-) between 1000 and 1350 cm^{-1}, which was evidence of the fluorosilane grafted to the surface of an Anodisc alumina ultrafiltration membrane.

13) Reverse selectivity was observed for CO_2 over H_2, N_2, CH_4 and n-C_4H_{10}. Selectivities were as high as 13.5 for CO_2/ n-C_4H_{10} and 10 for CO_2/CH_4.

14) An exponential decrease in the permeance of the HDFS membrane with kinetic diameter results from transport limited by size or shape. In addition, transport of CO_2 was found to be enhanced by surface diffusion.

15) It was concluded that the HDFS layer was not stable at elevated temperatures up to 353 K.

16) In comparison, the selectivities measured for CO_2 over H_2 and N_2 were similar for both the HDFS and ODS membranes. The most significant distinction in performance between the two membranes was the change in the order of selectivity for CO_2 to hydrocarbons. The $CO_2/n\text{-}C_4H_{10}$ selectivity was 0.107 for the ODS membrane and 13.5, or over 100 times higher, for the HDFS membrane.

The change in the order of selectivity for CO_2 with relation to hydrocarbons and the contrast in the primary mechanisms of transport was a convincing demonstration of the effect of surface modification on membrane performance.

5.1.3 *Separation of Xylene Isomers by Pervaporation*

17) Selectivities for o-xylene over p-xylene and m-xylene were observed for the HDFS, silicalite and ZSM-5 membranes, while the selectivity of the ODS membrane was close to unity.

18) The selectivities for o-xylene/p-xylene were 2.4 for the ZSM-5, 1.4 for silicalite and 1.5 for the HDFS membrane.

19) The Ar/SF_6 selectivities of the zeolite membranes were 2.5 for ZSM-5 and 28 for silicalite, which was not an indication of their selectivity during pervaporation of xylenes.

Though the selectivities of these membranes for o-xylene are not high, they are respectable for the separation of a mixture with a relative volatility that is close to one.

5.2 Recommendations

The following section describes recommendations for future work on the development of silane modified membranes and for the separation of xylene isomers by pervaporation.

5.2.1 *Silane Chemistry*

1) The most important step towards improving the performance of silane modified membranes is to gain a better understanding of the surface chemistry that is involved during silanization of porous materials.

2) During this research, the silanization technique was performed as described by Leger et al. [4]. In retrospect, Leger's description did not include crucial steps for surface hydroxylation and their explanation of the silane concentration used during membrane modification was confusing. The concentration of silane reactant used for this research was several times higher than that of other groups who have published results for silane modified membranes [4-6]. These factors may be responsible for the deposition of a 11 nm polymer layer as opposed to a monolayer of ODS, as described in Chapter 2. Also, selectivities and permeances were often higher than observed by other groups. It would be advantageous to improve reproducibility and gain control of thickness and morphology during deposition of the silane layer.

3) It is recommended that studies on deposition using ODS and HDFS be continued, because they are the most popular precursors studied in the development of packing materials for chromatography [7,8]. The effects of solvent type, temperature, silane concentration, and surface water during deposition of these films should be considered [9-13].

4) Atomic force microscopy (AFM) techniques should be refined to obtain more information about the microstructure of the silane layers. A few attempts were made to measure the thickness of the silane layer on polycrystalline sapphire disks. First we tried to etch a step into the silane layer by masking half of the sample with a silicon wafer and exposing it to a 1.25 milli-Watt/cm^2 UV light for 5.0 seconds (Optical Associates Inc., Model 28, Chelmsford, MA). Tapping mode AFM was performed using a Nanoscope III (Digital Instruments, Santa Barbara, CA) instrument to measure the height of the step, which is equal to the thickness of the silane layer. However, the step could not be located, and there

was no noticeable difference in the images that were generated compared to unmodified samples.

5) Organosilicon chemistry offers thousands of possible functional groups that are available commercially or can be synthesized. A thorough literature search on the development of stationary phases for chromatographic separations or separations using complexing agents would be a valuable resource for screening prospective functional groups.

5.2.2 *Transport through Silane Modified Membranes*

6) To improve the performance of silane modified membranes it is necessary to study the effects of competitive adsorption on transport and selectivity. Binary gas separation experiments should be performed over a range of temperatures and pressures. Binary gas separation phenomena should then be modeled using generalized Stefan-Maxwell (GSM) equations [2,14,15].

7) Models of adsorption, for the binary gas transport model, should be improved by applying the appropriate adsorption isotherms for specific gases; for example Langmuir adsorption, Henry's Law adsorption or perhaps an improvement in theory would be gained with the Dubinin-Radushkevitsch adsorption isotherm [2,3].

5.2.3 *Separation of Xylene Isomers by Pervaporation*

8) Since the selectivity of xylenes in these materials appears to be enhanced by interactions of the polar o-xylene molecule with the polar or polarizable surfaces of the ZSM-5 and HDFS membranes, it may be possible to improve the membrane performance through surface chemistry. Silane modification can be performed with numerous functional groups that may interact more strongly with specific xylene isomers. Also, ion exchange, say with Na^+, should have a significant influence on the selectivity of ZSM-5 for o-xylene.

9) In Chapter 4, it was suggested that the selectivity of xylenes appeared to be due to polar interactions between of o-xylene with the membrane. Molecular modeling is necessary to gain a better understanding of these phenomena. Specifically, Monte Carlo sorption simulations should be performed to see why ZSM-5 has a better selectivity for o-xylene/p-xylene than silicalite. These simulations should also be extended to sorption of o-xylene on ZSM-5 after ion exchange.

10) Observations from literature indicate that the feed concentration and the temperature at which pervaporation is performed has a significant affect on a membrane's selectivity for xylenes. It is recommended that future screening experiments cover a range in temperature from about 273 to 313 K [16].

5.3 References

1 J. W. Bakker, L. J. P. van den Broeke, F. Kapteijn, and J. A. Moulijn, *AICHE Journal* **43,** 2203-2214 (1997).

2 A. J. Burggraaf, in *Fundamentals of Inorganic Membrane Science and Technology*, edited by A. J. Burggraaf and L. Cot (Elsevier Science B.V., 1996), pp. 331-431.

3 A. J. Burggraaf, *Journal of Membrane Science* **155,** 45-65 (1999).

4 C. Leger, H. D. L. Lira, and R. Paterson, *Journal of Membrane Science* **120,** 187-195 (1996).

5 J. R. Miller and W. J. Koros, *Separation Science and Technology* **25,** 1257 - 1280 (1990).

6 P. Mejean, A. Collet, M. Viguier, A. Sivade, D. Bourret, and A. Larbot, in *ICIM 5* (Japan, 1998), pp. 176-179.

7 B. Buszewski, R. M. Gadzala-Kopciuch, M. Markuszewski, and R. Kaliszan, *Analytical Chemistry* **69,** 3277-3284 (1997).

8 M. Ho, M. Cai, and J. E. Pemberton, *Analytical Chemistry* **69,** 2613-2616 (1997).

9 R. Banga and J. Yarwood, *Langmuir* **11,** 4393-4399 (1995).

10 J. B. Brzoska, I. B. Azouz, and F. Rondelez, *Langmuir* , 4367-4373 (1994).

11 S. Kim and G. R. Gavalas, *Journal of Colloid and Interface Science* **161,** 6-18 (1993).

12 M. E. McGovern, K. M. R. Kallury, and M. Thompson, *Langmuir: the ACS journal of surfaces and colloids* **10,** 3607-3614 (1994).

13 C. P. Tripp and M. L. Hair, *Langmuir: the ACS journal of surfaces and colloids* **8,** 1120-1126 (1992).

14 J. O. Hirschfelder, C. F. Curtiss, and R. B. Bird, *Molecular Theory of Gases and Liquids* (John Wiley & Sons, New York, 1964).

15 J. C. Slattery, *Momentum, Energy and Mass Transfer in Continua*, second edition ed. (Robert E. Krieger Publishing Company, New York, 1981).

16 F. P. McCandless, *Ind. Eng. Chem. Prod. Res. Dev.* , 483-488 (1982).

Appendix 1

An Ab Initio Study of Surface Diffusion and Capillary Diffusion through Microporous Silica Membranes

Adsorption phenomena are responsible for the transport mechanisms involved in surface diffusion enhanced permeation and capillary diffusion of gases and *reverse selectivity*, or selectivity for heavy gases over lighter ones, through membranes [1-3]. Molecular modeling of the adsorption phenomena provides insight into the performance and development of these membranes. Understanding the interactions of gases with specific adsorption sites leads to the prospect of optimizing surfaces for chemical separations.

This chapter compares energies of adsorption of gases determined from quantum mechanical (QM) calculations for hydroxylated silica surfaces with the energies of adsorption estimated from gas transport data reported by Hassan and Heidrich [4-6]. The interactions of gases with isolated hydroxyl groups are considered the principal contributors to competitive adsorption and surface flow of silica surfaces [4-8].

A1.1 Background

A1.1.1 *Determination of Adsorption Phenomena with Permeance Measurements*

In microporous membranes the permeance (P) is an exponential function of temperature, as given below:

$$P = P_o e^{\left(\frac{-E^+}{RT}\right)} \qquad \text{(A1.1)}$$

where P_o is the preexponential factor, R is the gas constant, T is the experimental temperature, and E^+ is the apparent activation energy determined from the slope of an Arrhenius plot of permeance as a function of temperature. For microporous membranes in which configurational diffusion, or molecular sieving, is the primary transport mechanism, E^+ is proportional to the kinetic diameter of the diffusing gas.

If surface diffusion or capillary diffusion was present in parallel with configurational diffusion, then E^+ is reduced by adsorption. In this case, E^+ is equal to the difference between the intrinsic activation energy of diffusion (E_d) and the total energy of adsorption (Q^+) as given in equation A1.2:

$$E^+ = E_d - Q^+ \qquad \text{(A1.2)}$$

The definition of Q^+ depends on the type of adsorption phenomena that is involved for a particular transport process, however is typically equal to the isosteric energy of adsorption (Q_a). The isosteric energy of adsorption is defined as the energy of adsorption at constant surface concentration. Q_a is useful to characterize surface diffusion processes with low surface coverage, because it accounts for interactions of gases with specific adsorption sites on the surface of the membrane.

A1.1.2 *Previous Experiments with Microporous PPG Silica Hollow Fiber Membranes*

Way [9], Hassan [4,5] and Heidrich [6] have investigated the effect of configurational diffusion, surface flow and capillary condensation on silica surfaces using microporous hollow fiber silica membranes. They chose microporous hollow fiber silica membranes, because the fibers provide a model material to study configurational diffusion and the interactions of gases with a silica surface. The mean pore diameter of the fiber was estimated to be between 5.9 and 8.5 Å, and pure gas selectivities were as high as 350 for H_2/N_2 and 240 for H_2/CO_2 at 343 K.

The relationship between the E^+ of diffusion and kinetic diameter of several gases through the hollow fiber silica membranes is shown in Figure A1-1. With the exception of SO_2, all of the gases exhibited a linear relationship between E^+ and kinetic diameter. This linear relationship of E^+ with kinetic diameter, along with high pure gas selectivities indicated that configurational diffusion was the primary transport mechanism [4-6]. For comparison, the transport of SO_2 and Kr were investigated because these gases have a similar kinetic diameter of 3.6 A. For SO_2, E^+ was 4.29 kcal/mole, which is less than half that of Kr, 10.86 kcal/mole. In this case, the linear fit represents E_d, therefore the

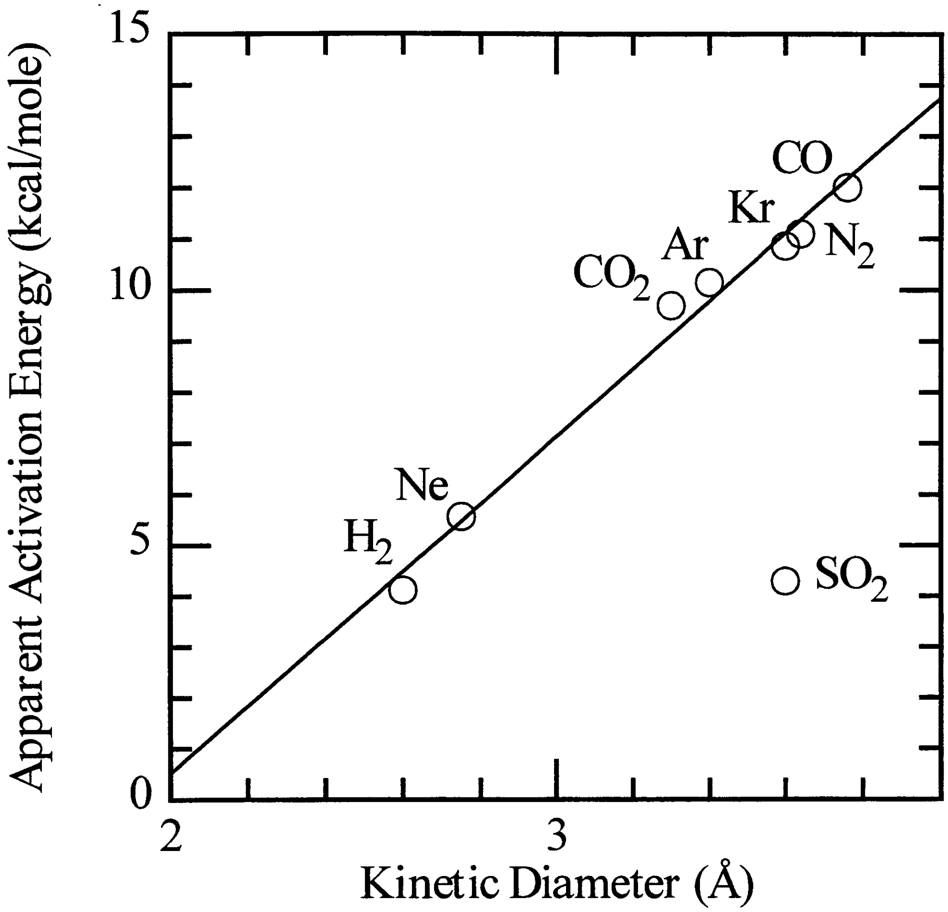

Figure A1-1: The apparent activation energy of diffusion through silica-hollow fiber membranes is a linear function of kinetic diameter for gases except SO_2 [4-6].

difference in E^+ for SO_2 from the linear fit predicted for gases in the configurational diffusion regime was equal to Q^+ attributed to capillary diffusion.

Further evidence of capillary diffusion resulted from permeance measurements by Heidrich [6]. Heidrich used a feed mixture of 5% SO_2 in He, because the vapor pressure of pure SO_2 was too low to provide the necessary driving force for significant permeation [6]. Without the use of a sweep gas, or carrier gas on the permeate side of the membrane, there was no measurable permeation observed for the mixture with a feed pressure of 20 bar. Therefore, SO_2 present in the feed was blocking the flow of He. A very low permeance of SO_2 was measured with a gas chromatograph when a He sweep gas was used. The low E^+ and low permeance were evidence of strong interactions (Q^+ is large) of SO_2 with the silica surface. This indicated that the adsorption of SO_2 resulted in capillary condensation, which blocked the flow of helium.

Hassan reported that the fibers achieved higher mixed gas selectivities than ideal selectivities for CO_2/CH_4 mixtures at temperatures below 373 K [4,5]. The CO_2/CH_4 mixed gas selectivities decreased from 250 at 298 K to 20 at 423 K, and were up to 40 % higher than selectivities calculated from pure gases below 373 K. The differences between the selectivities from mixtures and pure gas experiments were attributed to competitive adsorption where more strongly adsorbing gases hinder the surface diffusion of other gases in a mixture. A decrease in selectivity with temperature is often reported for microporous materials, because adsorption and surface flow are reduced when thermal energy (i.e., RT) becomes greater than the energy of adsorption [1,10-12].

Even though the increase in mixed selectivity for CO_2/CH_4 in mixed gases relative to the pure gas selectivity was significant evidence of adsorption and surface flow of CO_2, there was no decrease in E^+ observed in Figure A1-1. In this case, the adsorption energy of CO_2 on the microporous membranes was probably so small compared to E^+ that it was not resolved by this experiment.

In this section we have discussed experimental observations of surface diffusion of CO_2 and capillary diffusion of SO_2 through microporous hollow-fiber silica membranes. The next step was to use molecular modeling through quantum mechanical (QM) methods to investigate the interactions of Ar, N_2, CH_4, CO, CO_2, and SO_2 with a model silica surface. This enabled us to compare adsorption energies determined through QM calculations and from the transport data in Figure A1-1.

A1.2 Ab Initio Quantum Mechanical Calculations of the Energy of Adsorption

The isolated hydroxyl groups are considered to be the principal adsorption sites, or functional groups, responsible for surface diffusion on silica surfaces [4,8]. Simple surface clusters including silanol (H_3SiOH) and orthosilicic acid ($SiOH_4$) have been used to model the interactions of CO, H_2O, H_2, and H_2CO with hydroxyl groups on silica surfaces [8,13-16]. The complexes of adsorbates with these model surface clusters have been recently reviewed by Sauer and coworkers [16]. The literature indicates that either model of the isolated surface hydroxyl groups provides interaction energies, geometries, and vibrational modes that agree satisfactorily with experimental data. The silanol (H_3SiOH) cluster was chosen for this study to reduce the computer time required for these calculations, since processing time increases exponentially with the number of atoms (N), with the scaling factor[17] that lies between $N^{2.5}$ and N^4.

Calculations of Q_a required a series of steps to determine the optimized geometry and ground state energies for the surface model, the adsorbing species, and the van der Waals complex formed when the two interact [8,16,18]. Once the geometry of gas species and surface cluster were optimized, a scan of the potential energy surface was performed to locate the global minimum. The scan was performed by optimizing the geometry of the complex at the HF/3-21G* level of theory, and then performing several single point energy calculations as the adsorbing species was moved around the surface cluster. Basis set superposition errors (BSSE) were estimated using the counterpoise correction method [19]. Subsequently, frequency calculations at the desired temperature were performed to obtain thermal energy corrections. All calculations were performed using Mollier-Plesset perturbation theory truncated at the second order (MP2), and the standard 6-31+G** Pople basis sets were used [18]. The strategy for determining Q_a follows:

1. Geometry optimizations were performed for each molecule separately. The ground state energy (E^0) of each was computed at 0 K.

2. A geometry optimization was performed for the structure of the complex and the BSSE is determined for the complex.

3. Frequency calculations were performed at the desired temperature to compute the thermal energy (E^{th}).

4. Q_a was calculated in the following manner:

$$\Delta E^{o} = \Delta E^{o}_{\text{complex}} - [E^{o}_{silanol} + E^{o}_{gas}] + \text{BSSE} \qquad (A1.3)$$

$$\Delta E^{th} = E^{th}_{complex} - [E^{th}_{silanol} + E^{th}_{gas}] \qquad (A1.4)$$

$$Q_a = -\Delta E^{o} - \Delta E^{th} + \mathrm{R}T \qquad (A1.5)$$

where RT equals the work term $-\Delta(pV)$ since 1 mole of gas is lost to adsorption [17,18].

Calculations were performed at Colorado School of Mines using IBM RS/6000 model 380 and 580 workstations, with electronic structure programs Gaussian 92 [20], Gaussian 94 [21] and SPARTAN [22].

A1.3 Results and Discussion

The interactions of Ar, N_2, CH_4, CO_2, CO and SO_2 with a model surface, silanol, were studied using ab initio QM methods described in section A1.2. The geometry of each species was optimized, then the potential energy surface for each complex was scanned, through a series of single point energy calculations at the HF/3-21G* level, for the lowest energy conformation. The structure of each van der Waals complex was then optimized at the MP2/6-31+G** level, as shown in Figure A1-2.

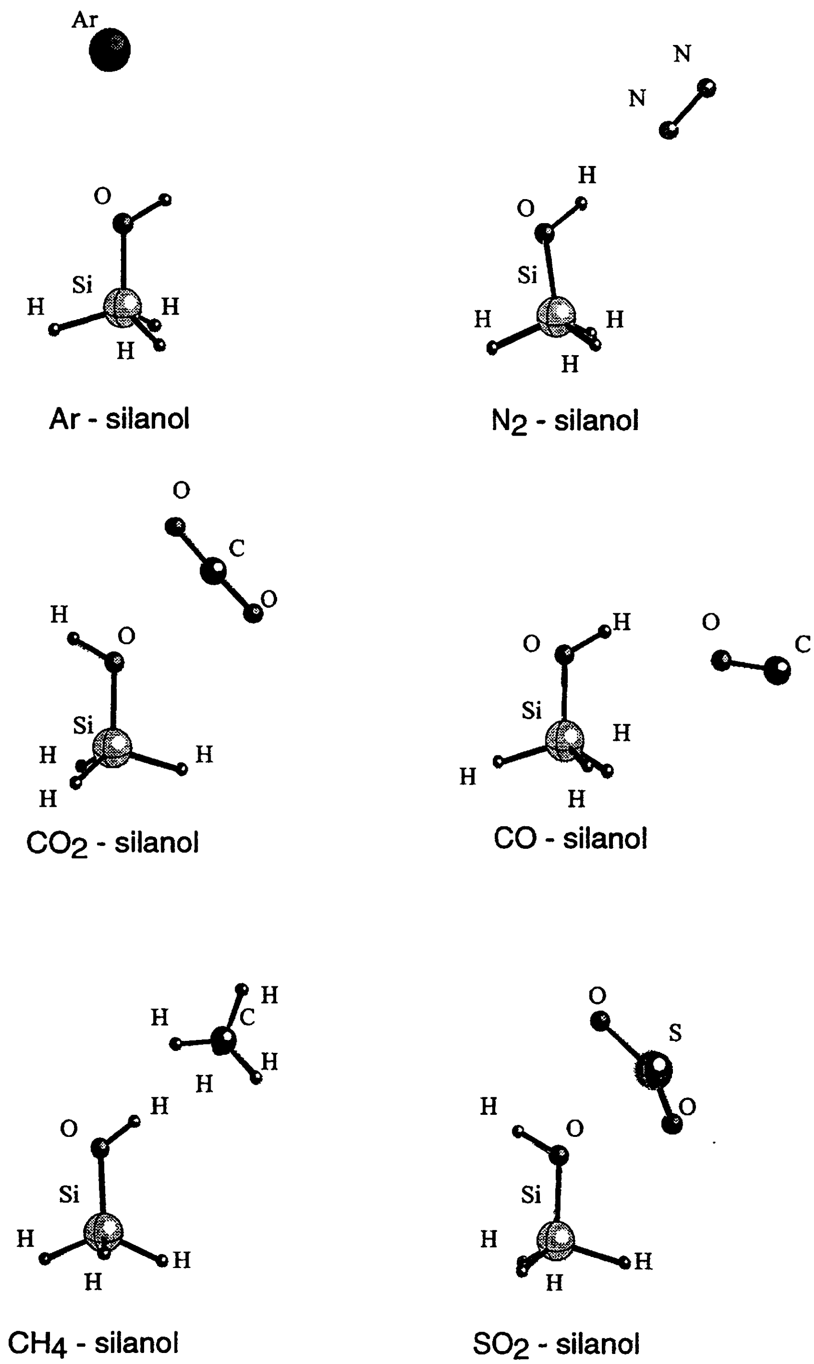

Figure A1-2: Ball and stick models of the optimized complexes.

Table A1-1 presents the results of the calculations, performed at the MP2/6-31+G** level of theory, used for estimating the enthalpy of adsorption for each species. The BSSE's were used to correct the ΔE^{o}. The ΔE^{th}'s were calculated at 370 K for comparison to the values of E^{+} that were determined from Arrhenius plots over a range of temperature from 298 K to 473 K [4,6].

Table A1-1: Energies of adsorption calculated for the ΔE^{o} with the silanol surface model. All calculations were performed at MP2/6-31+G** level of theory. All energies are given in kcal/mole. The ΔE^{th}'s were calculated at 370 K.

Sorbate	ΔE^{o}	BSSE	ΔE^{o} +BSSE	ΔE^{th}	Q_a @ 370 K
Ar	-0.705	-0.791	0.086	0.65	0.00
N_2	-2.12	0.98	-1.14	1.35	-0.52
CH_4	-1.12	0.70	-0.42	2.21	-1.09
CO	-1.58	0.92	-0.66	1.88	-0.48
CO_2	-4.03	1.84	-2.19	2.62	0.30
SO_2	-5.90	2.61	-4.50	2.36	2.88

SO_2 and CO_2 were the only gases for which positive Q_a's were calculated at 370 K, therefore these were the only gases that were predicted to adsorb onto the hydroxyl groups on the surface of silica under these conditions. The thermal energy of the other gases were much higher than the *zero point energies* (ΔE^{o} +BSSE). By means of equation (A1.5), there is a sign change between the zero point energies and Q_a. For all of the calculated zero point energies listed in Table A1-1 that are negative (repulsion), Q_a for the respective gas would become positive at sufficiently low temperatures predicting adsorption onto the silanol surface model. Argon is a noble gas and is not expected to interact strongly with any surface and was not predicted to interact with the silanol molecule.

Characteristics of an adsorbed phase and surface interactions can be gained from a comparison of Q_a to the available thermal energy (RT). If $RT >> Q_a$, then the adsorbed molecules behave like a two-dimensional fluid, or a mobile adsorbed gas phase, at low surface concentrations. If $RT << Q_a$, then localized adsorption that occurs at higher surface concentrations. As shown in Figure A1-3, the calculated Q_a for CO_2 was in the region of low surface concentration at 370 K, and the calculated Q_a for SO_2 was in the region of localized adsorption at 370 K [10,23].

The Q_a calculated for SO_2 was about an order of magnitude higher than for CO_2, which was consistent with the adsorption behavior observed during transport experiments and the fact that SO_2 is the only condensable gas under these conditions. The critical temperatures of 430.7 K for SO_2 and 304.2 K for CO_2 are significantly higher than the critical temperature of 190.7 K for methane, which is the next most condensable gas [24]. The sorption predicted by the calculated Q_a, and the fact that CO_2 is close to its critical

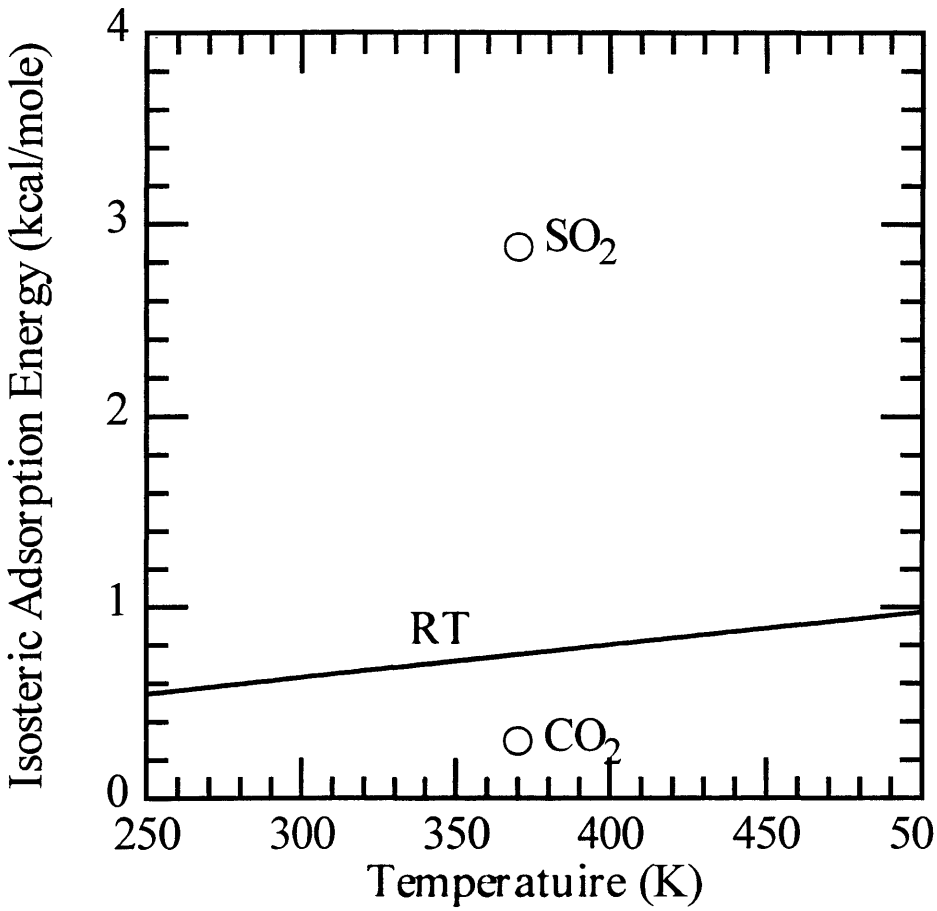

Figure A1-3: Isosteric energy of adsorption (Q_a) relative to the thermal energy (*RT*, solid line) as function of temperature. The region above *RT* includes localized adsorption that occurs at higher surface concentrations. The region below *RT* includes mobile two-dimensional gas phases at low surface concentrations.

temperature relative to CH_4, was consistent with the competitive adsorption and surface diffusion observed for CO_2 in this mixture (section A1.1.2).

In the absence of transport mechanisms other than configurational diffusion, surface diffusion and capillary diffusion, the total energy of adsorption, or condensation, (Q^+) contributed to transport can be determined from equation (A1.2) using the transport data shown in Figure A1-1. For example, E^+_{pred} predicted for SO_2 from the linear fit as a function kinetic diameter in Figure A1-1 was 11.16 kcal/mole, and the measured E^+ was 4.29 kcal/mole. The difference between the predicted and measured values for E^+ is equal to $Q^+_{\exp}$, as shown below:

$$Q^+_{\exp} = E^+_{pred} - E^+ \qquad \text{(A1.6)}$$

The value $Q^+_{\exp}$ for SO_2 in this example was 6.87 kcal/mole, which compares very well with the literature values for Q_a on silica materials, listed in Table A1-2.

Table A1-2: Energies of adsorption for SO_2 on two porous silica materials.

Adsorbate	**Sorbent**	**Temp. (K)**	**Q_a (kcal/mole)**
SO_2	Vycor Glass [25]	288 – 303	5.5 - 8.3
	Silica gel [2]	313	6.730
		303	6.940

The value of $Q^{+}_{\exp}$ determined for SO_2, from the example above, was 3.99 kcal/mole higher than the calculated Q_a, from Table A1-1. The difference between $Q^{+}_{\exp}$ and Q_a, along with the observation that SO_2 blocked the transport of He (section A1.1.2), was an indication that the diffusion of SO_2 is not in the gas phase. Therefore, the total contribution of adsorption in the presence of capillary condensation must account for the energy evolved from condensation, or the negative of the heat of evaporation (ΔH_v), as given in equation (A1.7):

$$Q^{+}_{theory} = Q_a + \Delta H_v \qquad \text{(A1.7)}$$

Table A1-3 includes an estimation of Q^{+}_{theory} from equation (A1.7) using the calculated value of Q_a and a value for ΔH_v taken from literature [26]. There was a 7.7% error for Q^{+}_{theory} that indicated reasonable agreement with $Q^{+}_{\exp}$. This was consistent with the hypothesis that capillary diffusion was responsible for the low E^{+} observed in Figure A1-1. The agreement between experiment and the model of adsorption on the model silica surface is also evidence that isolated hydroxyl sites on silica are responsible for the enhanced diffusion of SO_2.

Table A1-3: The contribution of adsorption estimated from equation (A1.7).

Adsorption Parameter	(kcal/mole)
Q_a (calculated)	2.88
$-\Delta H_v$ (from literature) [26]	4.52
Q^{+}_{theory} Equation (A1.7)	7.40
$Q^{+}_{\exp}$ Equation (A1.6)	6.87 kcal/mole
% Error	7.7 %

The interactions between gases and the silanol surface model, predicted by QM calculations were in agreement with the experimental observations of surface diffusion of CO_2 and capillary diffusion of SO_2 through hollow fiber silica membranes. This supports the validity of the silanol clusters as a model silica surface and the participation of hydroxyl groups in surface diffusion and capillary diffusion of CO_2 and SO_2.

A1.4 Conclusions

Ab initio QM calculations were performed to model the adsorption of gases on a hydroxylated-silica surface. Isosteric energies of adsorption were determined via the QM calculations for Ar, N_2, CO, CO_2, CH_4 and SO_2 using silanol (H_3SiOH) as a model surface. SO_2 and CO_2 were predicted to adsorb onto a hydroxylated silica surface at 370 K. A Q_a of zero for Ar was calculated, and negative energies of adsorption (repulsion) were predicted for the other light gases at 370 K. The Q_a predicted for SO_2 (2.88 kcal/mole) was an order of magnitude larger than Q_a predicted for CO_2 (0.30 kcal/mole).

Previously reported mass transport experiments showed that configurational diffusion was the primary transport mechanism through microporous hollow-fiber silica membranes. However, the competitive adsorption and surface diffusion of CO_2 and capillary diffusion of SO_2 were observed. The interactions predicted for CO_2 were in agreement with the experimental observation of surface diffusion. The calculated Q_a of 0.30 kcal/mole was consistent with the adsorption of a two-dimensional gas phase at low surface concentrations.

A value for $Q^+_{\exp}$ (6.87 kcal/mole) was estimated using transport data from the hollow fiber silica membranes. An error of 7.7 % for Q^+_{theory} compared to $Q^+_{\exp}$ appeared to be consistent with the observation of capillary diffusion of SO_2 and supports the validity of the hydroxylated-silica model surface used for QM calculations. The calculated Q_a of 2.88 kcal/mole was consistent with localized adsorption that occurs at higher surface concentrations.

Molecular modeling via QM methods has provided useful insight into the mechanisms of transport on silica surfaces. During this investigation a simple hypothetical surface cluster, silanol, was used successfully to model adsorption on a silica surface. The effects of molecular interactions had a significant effect on the performance of the hollow fiber silica membrane.

A1.5 Nomeclature

BSSE	basis set superposition error
E^o	ground state energy
E^{th}	thermal energy
E^+	apparent activation energy
E_d	intrinsic activation energy of diffusion
ΔH_v	heat of evaporation
P	permeance
P_o	pre-exponential factor for permeance
p	pressure
Q^+	total energy of adsorption
Q_a	isosteric energy of adsorption
R	gas constant
T	temperature

A1.6 References

1 A. J. Burggraaf, in *Fundamentals of Inorganic Membrane Science and Technology*, edited by A. J. Burggraaf and L. Cot (Elsevier Science B.V., 1996), pp. 331-431.

2 E. R. Gilliland, R. F. Baddour, G. P. Perkinson, and K. J. Sladek, *Ind. Eng. Chem., Fundamentals* **13,** 9599 (1974).

3 M. B. Rao and S. Sircar, *Journal of Membrane Science* **85,** 253-264 (1993).

4 M. H. Hassan, Ph.D., Oregon State University, 1994.

5 M. H. Hassan, J. D. Way, P. M. Thoen, and A. C. Dillon, *Journal of Membrane Science* **104,** 27-42 (1995).

6 K. E. Heidrich, M.Sc., Colorado School of Mines, 1995.

7 T. Okubo and H. Inoue, *AICHE Journal* **35,** 845-848 (1989).

8 P. Ugliengo, V. R. Saunders, and E. Garrone, *Chem. Phys. Lett.* **196,** 501-508 (1990).

9 J. D. Way and D. L. Roberts, *Separation Science & Technology* **27,** 29-41 (1992).

10 T. L. Hill, *An Introduction to Statistical Thermodynamics* (Addison-Wesley Publishing Company, Inc., Reading, 1960).

11 S.-T. Hwang and K. Kammermeyer, *Membranes in Separations* (John Wiley and Sons, New York, 1975).

12 J. Kärger and D. M. Ruthven, *Diffusion in Zeolites and Other Microporous Solids* (John Wiley and Sons, New York, 1992).

13 W. B. D. Almeida and P. O'Malley, *J. Chem. Soc. Faraday Trans.* **89,** 983-989 (1993).

14 S. H. Garofalini, *Journal of Non-Crystalline Solids* **120,** 1-12 (1990).

15 E. Garrone, V. B. Kazansky, L. M. Kustov, J. Sauer, I. N. Senchenya, and P. Ugliengo, *J. Phys. Chem.* **96,** 1040-1045 (1992).

16 J. Sauer, *J. Phys. Chem.* **91,** 2315-2319 (1987).

17 J. B. Foresman and A. Frisch, *Exploring Chemistry with Electronic Structure Methods* (Gaussian, Inc., Pittsburgh, 1993).

18 W. J. Hehre, L. Radom, P. V. R. Schleyer, and J. A. Pople, *Ab-Initio Molecular Orbital Theory* (Wiley, New York, 1986).

19 S. F. Boys and F. Bernardi, *Molecular Physics* **19,** 553-566 (1970).

20 Gaussian, , F2 ed. (Gaussian, Inc., Pittsburgh, PA, 1992).

21 I. Gaussian, (Gaussian, Inc., Pittsburgh, 1994).

22 SPARTAN, , 3.1 ed. (Wavefunction, Inc., Irvine, CA 92715, 1994).

23 T. L. Hill, *The Journal of Chemical Physics* **25,** 730-735 (1956).

24 *Lange's Handbook of Chemistry*, Vol. , edited by J. A. Dean (McGraw-Hill Book Company, New York, 1979).

25 S. Brunauer, *The adsorption of gases and vapors* (Oxford University Press, Milford, 1943).

26 *Perry's Chemical Engineering Handbook*, Sixth ed. (McGraw-Hill Book Company, New York, 1984).

Appendix 2

Modeling of Separations through a Shell and Tube Membrane Module

A2.1 Derivation of the Shell and Tube Model

A model was developed to predict the concentration (partial pressure) profile along the length of a tubular membrane for separations of n-C_4H_{10}/N_2 and C_4H_{10}/CO_2 that were limited by the available partial pressure diving force. Integral analysis of the molar flow rates of each species on the tube (feed, F_i) side and the shell side (permeate, Q_i) of the membrane was used to model partial pressure as a function of axial position (x), along the length of the membrane [1]. The tube side differential material balance on species i in a countercurrent or cocurrent flow module was:

$$\frac{\mathrm{d}F_i}{\mathrm{d}x} = -\frac{A}{L}\overline{P_i}\left[\frac{F_i}{F_T}p_F - \frac{Q_i}{Q_T}p_P\right] \tag{A2.1}$$

A similar relationship was given for the shell side below:

$$\frac{\mathrm{d}Q_i}{\mathrm{d}x} = \frac{A}{L}\overline{P_i}\left[\frac{F_i}{F_T}p_F - \frac{Q_i}{Q_T}p_P\right] \tag{A2.2}$$

In this model an average permeance ($\overline{P_i}$)for each component was assumed for a tube of total length L and total membrane surface area A. The subscripts T, F and P are for total flow rates, feed pressures and permeate pressures respectively. The boundary conditions for equations (A2.1) and (A2.2) with cocurrent flow were:

$$F_i = F_{io} \text{ at } x = 0 \tag{A2.3}$$

$$Q_i = Q_{io} \text{ at } x = 0 \tag{A2.4}$$

Analytical expressions derived for $F_i(x)$ and $Q_I(x)$ by solving the material balance and boundary condition equations are given below:

$$F_i(x) = e^{(-a(1+b)x)}\left[\frac{be^{(a(1+b)x)}(F_{io}+Q_{io})}{1+b} - \frac{-F_{io}+bQ_{io}}{1+b}\right] \tag{A2.5}$$

and

$$Q_i(x) = e^{(-a(1+b)x)}\left[\frac{e^{(a(1+b)x)}(F_{io}+Q_{io})}{1+b} + \frac{-F_{io}+bQ_{io}}{1+b}\right] \tag{A2.6}$$

Where constants a and b were introduced for mathematical convenience, as defined below:

$$a = \frac{A\,p_F}{L\,F_T}\overline{P_i} \tag{A2.7}$$

and

$$b = \frac{p_P F_T}{p_F Q_T} \tag{A2.8}$$

This solution is valid using an expression for the flow rate of a single species, because its application is restricted to binary gas separations.

A2.2 Prediction of Concentration Profile in Shell and Tube Module

A plot of the predicted partial pressure of n-C_4H_{10} versus axial position with cocurrent flow in during a n-C_4H_{10}/N_2 separations experiment is given in Figure A2-1. Model parameters, listed in Table A2.1, were determined from experimental conditions. The compositions were known in the feed stream at $x = 0$, and for the feed and permeate streams at $x = L$, and pure gas permeances were used as conservative estimates. The flow rate (or partial pressure) at position $x = 0$ in the permeate stream was determined from the model. Under these conditions the model predicts that the difference in $p_{(n-C_4H_{10})}$ between the feed and permeate streams was ≈ 0.03% at midpoint (2.0 cm) along the length of the membrane. The upper limit of selectivity occurs under the conditions when $p^P_{n-C_4H_{10}} = p^R_{n-C_4H_{10}}$, therefore it was possible to achieve selectivities that were artificially lower for mixed gases than for pure gases under these conditions.

The results presented in Figure A2-1 are also representative of the concentration profile in the module during the n-C_4H_{10}/CO_2 separations experiment. In this case it was not intuitive that driving force limitations would occur, because the n-C_4H_{10}/CO_2 selectivity was less than 1/3 the selectivity of n-C_4H_{10}/N_2. However, the total flux through the membrane was 2.9 times higher for the n-C_4H_{10}/CO_2 experiment, thus permeating more butane relative to the amount available in the feed. Increasing both the feed flow rate and the total feed pressure are recommended to avoid driving force limitations in both cases.

Table A2-1: Parameters used in the integral analysis of n-C_4H_{10} separations from N_2 as a function of the axial position along the length of the membrane. The analysis was used to estimate the mean permeance of n-C_4H_{10} and an upper limit for the selectivities during these separations.

Parameters	**n-C_4H_{10}/N_2**
A (cm^2)	8.79
L (cm)	3.99
F_T (scc/min)	38.9
Q_T (scc/min)	1.85
p_F (psia)	32.09
P_P (psia)	17.09
Feed - mole fraction n-C_4H_{10}	0.2160
Permeate - mole fraction n-C_4H_{10}	0.3840
$\overline{P}_{(N_2 \text{ or } CO_2)}$ ($scc \cdot cm^{-2} \cdot s^{-1} \cdot cmHg^{-1}$)	1.15×10^{-5}
$\overline{P}_{(n-C_4H_{10})}$ ($scc \cdot cm^{-2} \cdot s^{-1} \cdot cmHg^{-1}$)	5.54×10^{-4}

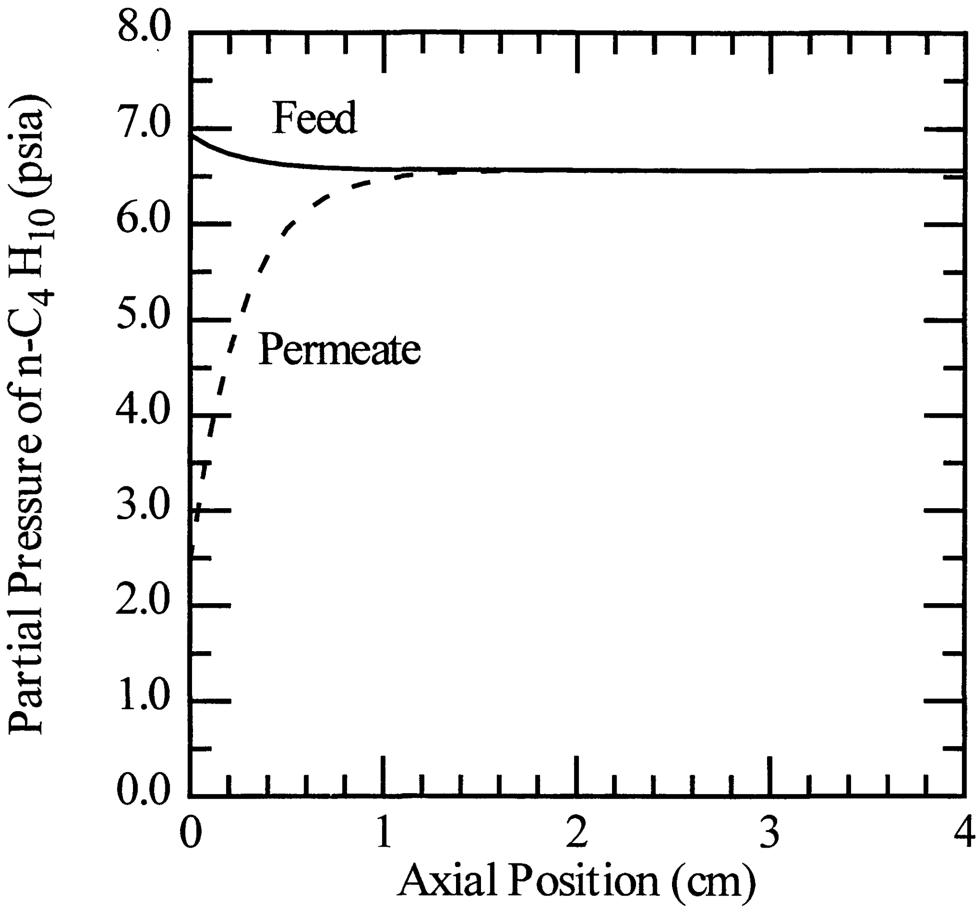

Figure A2-1: The predicted concentration profile of n-C_4H_{10} as a function during mixed gas separations with N_2.

A2.3 Nomenclature

A	membrane surface area
F	feed flow rate of species
F_T	total feed flow rate
L	total length of the tube
p	pressure
$\overline{P_i}$	mean permeance for species i
Q	permeate flow rate
T	temperature
x	length coordinate

Indices

F	feed
o	at $x = 0$
P	permeate
T	total

A2.4 References

1 J. P. Collins, J. D. Way, and N. Kraisuwansarn, *Journal of Membrane Science* **77**, 265-282 (1993).

Appendix 3

Procedures for the Operation of the Hewlett Packard 5890 Series II Gas Chromatograph using ChemStation Software

This is a summary of the procedures for operation of the Hewlett Packard 5890 Series II Gas Chromatograph (GC) using ChemStation Software. The GC is set up with a 20' Alltech Haysep-Q column using approximately 44.0 psig He sweep at 50 °C. A ten port Valco sample valve was used to sample the permeate and residue streams from a membrane. The valve was switched between by running two *methods*, or ChemStation routines, in series. Several runs were set up in series by alternating methods repeatedly with a ChemStation *sequence*. A printout of one of the ChemStation set up to sample the permeate stream is provided below. The method for sampling the residue stream is identical except for the initial setting for valve 1.

Method Information

Permeate: Analysis of mixtures of butane and light gases

Run Time Checklist

```
       Pre-Run Cmd/Macro:  off
        Data Acquisition:  on
  Standard Data Analysis:  on
```

Customized Data Analysis: off

Save GLP Data: off

Post-Run Cmd/Macro: off

Save Method with Data: off

OVEN\DET

Runtime (min): 39.0

Zone Temperatures:

	State	Setpoint
Inl. A	ON	120 C.
Inl. B	ON	120 C.
Det. A	ON	225 C.
Det. B	ON	225 C.
Aux.	OFF	50 C.

Oven Zone:

Oven max	230 C.
Equib Time	3.00 Min.
Oven State	ON
Cryo State	OFF
Ambient	20 C.
Cryo Blast	ON

Oven Program:

	Setpoint
Initial Temp.:	50 C.
Initial Time:	5.0 Min.

Level	Rate (C/min.)	Final Temp.(C)	Final Time (min)
1	50.0	50	5.00
2(A)	50.0	200	15.0
3(B)	50.0	50	10.0

Purge Valve Settings

Purge A/B

	Init Value	On Time (Min.)	Off Time (Min.)
A (Valve 3)	Off	0.00	0.00
B (Valve 4)	Off	0.00	0.00

A - Splitless Injection:	No
B - Splitless Injection:	No

Valves/Relays Information

Initial Setpoints:

5890 Valves:

Valve 1:	On
Valve 2:	Off
Valve 3 (Purge A):	Off
Valve 4 (Purge B):	Off

Valve/Relay Time Table:

Time	Name	State	Comment
0.00	Valve 1	Off	

Detector Information

Detector A:

Type	FID
State	OFF

Detector B:

Type	TCD
State	ON

Timed Events:

Events:	Value:	Time:
Initial TCD B Sensitivity	High	Initial
Initial TCD B Polarity	+	Initial

Signal Information

Save Data: Signal 1

Signal 1:

Signal	Det. B
Data rate	5.000 Hz.
Peakwidth	0.053 min.
Start Time	0.00 min.
Stop Time	650.00 min.

Signal 2:

Signal	Testplot
Data rate	5.000 Hz.
Peakwidth	0.053 min.
Start Time	0.00 min.
Stop Time	650.00 min.

Appendix 4

Operating Procedures for Gas Chromatograph-Mass Spectrometer

This is a description of the procedures used to analyze the composition of mixtures of xylene isomers using a Hewlett Packard 5890 gas chromatograph with a Hewlett Packard 5970 mass spectrometer (GC-MS). A 30 m long Alltech EC-WAX silica capillary column with an inner diameter of 0.25 mm was used with He (Grade 5.0) sweep gas.

A4.1 Start-Up Procedures

1. Make sure there is He (Grade 5.0) sweep gas to sample loop.
   a. Feed pressure = 40 psig
2. Make sure that there is adequate vacuum before taking turbo pump off of standby.
   a. Heater should be on already and backing pump should be running
   b. Needle on vacuum gauge should to the right of center

NOTE: Backing (mechanical) pump must be on at all times, especially when mass spec is taken off of standby mode. Turbo speed pump indicator should move all of the way to the right, in the green, when taken off of standby mode.

3. Take mass spec off of standby (push standby button in)

    a. Heater light goes off for a minute and then standby light goes off

4. Turn on oven temperature to 30° C

5. Turn on det (detector) B temperature to 200°

6. Turn on inj (injector) B temperature to 250° C

7. Helium sweep pressure set to approx. 5 psig with just a bubble coming from the split.

8. Turn on computer

    a. Switch in back of monitor

    b. Switch for hard-drive left-front

9. Set up for run

    a. Set the date and time

    b. Tune (at least once a day)

        [utility] → [autotune] - using K-keys

        [full autotune] . . . open calibration valve on left side

        [enter] -may give an error message

        [exit]. if everything is OK, it will tune despite error message

    c. Print out report of calibration and put into notebook (make sure to label with date)

    d. Close calibration valve → [enter] → [quit]

    e. Look at background

10. Data acquisition

a. [data acquisition]→ [load store parameters] → [load parameter]

*correct filename for method to analyze xylene mixtures = msparam.a

b. [prep to inject]

*Use a 0.10 μ l sample after rinsing syringe 10 times to clear old sample out

c. pick a name for the data output file → ([GO] or push start button on GC)

(example of good file name: feed 5-25-99 file kcm52599)

d. after run → [exit] → [quit]

11. Data editing [date editor] → [total ion chromatogram]

a. integration: to perform [chromo keys] → [run integ]

to get list [list int results]

b. for unknown chromatographs:

[spectrum keys] → [more keys] → [pbm search] → nbs43.k

12. **Extra tips:**

a. If you don't know file name type "?" and it will give you a list

b. For next sample: go back to [prep to inject]

13. **Trouble Shooting:**

a. Splitter: splitter should be set to 50 cc/min. Test using bubble flow meter. If not correct, turn knob directly over splitter, but no other knob.

b. Purge from septum needs to be non-zero

A4.2 Shut-Down Procedure

1. Turn down flow through splitter until it is just a bubble. As long as there is a little flow, it is ok.
2. Go to top of menu for GC software application and then turn off the monitor and hard drive.
3. Put turbo-pump on standby.
4. Turn off heating zones in GC
   a. oven
   b. detector
   c. injection port

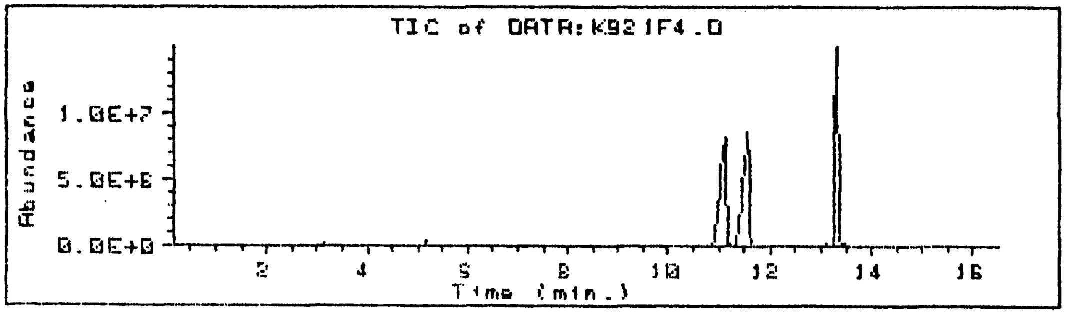

TIC of DATA:K921F4.D 4 integration peaks found.

Peak#	Ret Time	Type	Width	Area	Start Time	End Time
1	5.180	BB	0.042	7274443	5.108	5.264
2	11.111	BV	0.131	747784062	10.803	11.268
3	11.551	VV	0.141	742089238	11.268	11.894
4	13.324	PV	0.060	551244961	13.183	13.702

Figure A4-1: Sample chromatograph for analysis of a mixture of xylene isomers. The order of elution is p-xylene, m-xylene and o-xylene.